Lithos 346–347 (2019) 105151

Contents lists available at ScienceDirect

Lithos

journal homepage: www.elsevier.com/locate/lithos

Late Paleocene adakitic granitoid from NW Iran and comparison with adakites in the NE Turkey: Adakitic melt generation in normal continental crust

Hossein Azizi [a,*], Robert J. Stern [b], Gültekin Topuz [c], Yoshihiro Asahara [d], Hadi Shafaii Moghadam [e]

[a] Department of Mining Engineering, Faculty of Engineering, University of Kurdistan, Sanandaj, Iran
[b] Geosciences Department, University of Texas at Dallas, Richardson TX75083-0688, USA
[c] Istanbul Technical University, Eurasian Institute of Earth Sciences, Ayazağa, 34469 Istanbul, Turkey
[d] Department of Earth and Environmental Sciences, Graduate School of Environmental Studies, Nagoya University, Nagoya 464-8601, Japan
[e] School of Earth Sciences, Damghan University, Damghan 36716-41167, Iran

ARTICLE INFO

Article history:
Received 21 March 2019
Received in revised form 9 June 2019
Accepted 22 July 2019
Available online 26 July 2019

Keywords:
High potassium granite
Continental adakite
Crustal melting
Iran
Pontides
Turkey

ABSTRACT

Late Paleocene adakitic granitoids are rare in Iran except in the northwest. We focused on the adakitic Saqqez-Takab pluton, which occupies an area of ~600 km^2. New U-Pb zircon dating yield crystallization ages of 58–56 Ma (Thanetian). These granitoids comprises granite, quartz monzonite and monzogranite with granular to mylonitic textures. They have high SiO_2 abundances (59.1–78.6 wt%), high ratios of Sr/Y (50–490) and La/Yb ratios (19–237), along with high Ba (779–2466 ppm) and light rare earth element contents (e.g., La = 11–70 ppm). Saqqez-Takab granitoids have compositions that are similar to high-silica adakites, including low Mg- number (Mg# < 0.5), TiO_2 (<0.93 wt%), Cr (<38 ppm) and Ni (<55 ppm). K_2O/Na_2O ratios of these granitoids are high (>0.7), resembling K-rich adakitic granitoids. Initial ratios of $^{87}Sr/^{86}Sr$ and $\varepsilon_{Nd}(t)$ vary from 0.7044 to 0.7053 and −2.8 to +2.0 respectively. These isotopic signatures differ from those of typical subducting slab-derived adakites (O-type adakite) with high positive $\varepsilon_{Nd}(t)$ and from collision-related adakites (C-type adakite) with negative $\varepsilon_{Nd}(t)$. The geochemical and isotopic characteristics of Saqqez-Takab granitoids are most consistent with magma being produced by amphibole-dominated fractionation of hydrous melts of subcontinental lithospheric mantle accompanied by minor assimilation of lower mafic calc alkaline continental crust. Distribution of similar-ages adakites in the NW Iran and E Pontides of Turkey suggests that these melts formed similarly. Upwelling of hot asthenosphere due to Neotethys slab rollback led to partial melting of lower continental crust calc alkaline mafic rocks and/or amphibole fractionation from mafic magma produced K-rich adakitic rocks in eastern Turkey and NW Iran during the late Paleocene.

1. Introduction

Adakite is commonly used to describe felsic igneous rocks with high Sr/Y and La/Yb ratios. Since the term was first coined in 1990 (Defant and Drummond, 1990), adakites have been a topic of research (e.g., Castillo, 2006; Condie, 2005; Hastie et al., 2010; Martin, 1999). Martin et al. (2005) subdivided these into low-silica (LSA) and high-silica adakites (HSA). Adakites are further subdivided into sodic (K_2O/Na_2O < 0.6; Defant and Drummond, 1990) and potassic varieties (K_2O/Na_2O > 0.6; Xiao and Clemens, 2007). Residues or cumulates of garnet, amphibole, and rutile and absence of plagioclase in the source rocks mainly control the chemical composition of adakitic melts. The roles of one or more of these minerals during magma genesis and evolution can explain the high contents of the light rare earth elements (LREEs) and low contents of the heavy rare earth elements (HREEs) in adakitic melts.

Based on the stability of these minerals, two main processes are proposed for adakite genesis: (a) partial melting of hot, young subducting oceanic crust, metamorphosed to eclogite or amphibolite (Defant and Drummond, 1990; Martin et al., 2005), and (b) partial melting of lower continental crust in the garnet stability field (deeper than 50 km) (e.g. Chung et al., 2003; Coldwell et al., 2011). Additional processes such as partial melting of metasomatized mantle, partial melting of lower crust granulites (Li et al., 2017), amphibole (+ rutile + titanite) -dominated differentiation or partial melting (e.g., Liu et al., 2010; Martin et al., 2005; Moyen, 2009), crustal assimilation (Castillo et al., 1999), delamination of lower crust and melting in underlying hot mantle (Stern and Kilian, 1996; Martin et al., 2005; Li et al., 2013; Qian and Hermann, 2013;), remelting of arc basalts at high pressure

* Corresponding author.
E-mail address: azizi1345@gmail.com (H. Azizi).

https://doi.org/10.1016/j.lithos.2019.105151
0024-4937/

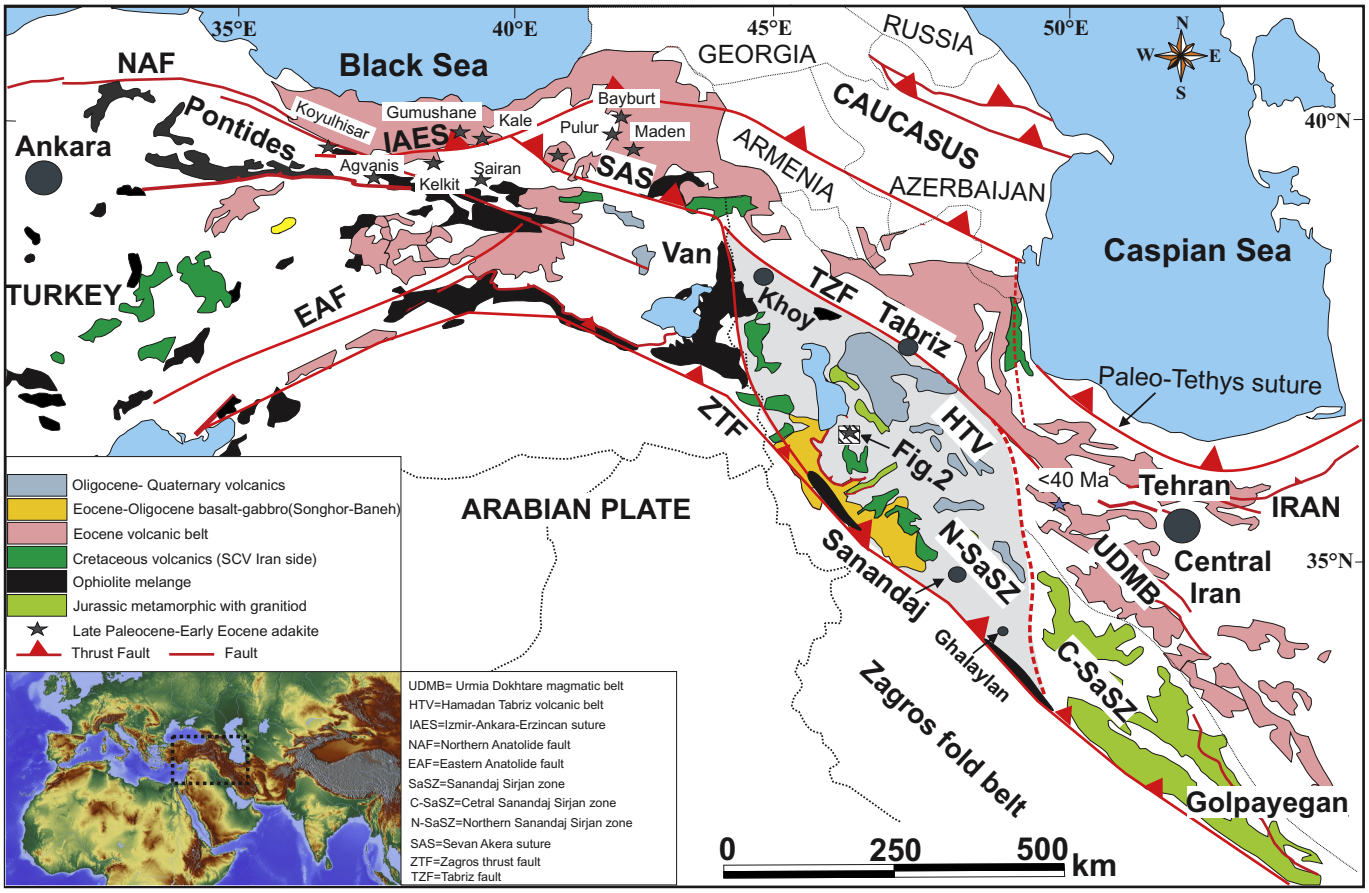

Fig. 1. Simplified geology map of northwest Iran and eastern Turkey (Modified from Topuz et al., 2005, 2011; Azizi and Jahangiri, 2008; Azizi and Moinevaziri, 2009; Karsli et al., 2010; Eyüboglu et al., 2011; Nouri et al., 2016). Stars show the distribution of late Paleocene- early Eocene adakites in northwest Iran and eastern Turkey.

are also suggested. Adakites occur in various tectonic environments, ranging from Archean tonalite-trondhjemite-granodiorite rocks (TTG) (>3.5 Ga) to present-day hot subduction and post-collisional settings. Adakites are thus keys for understanding Earth history and geodynamics of orogenic belts.

Adakitic rocks have been reported from northwest, central and northeast Iran (e.g., Azizi et al., 2014; Delavari et al., 2014; Ghorbani and Bezenjani, 2011; Jahangiri, 2007; Omrani, 2018; Rossetti et al., 2014). In the Sanandaj-Sirjan zone (SaSZ), Jurassic (157 Ma) granitoids with adakitic and tonalite-trondhjemite-granodiorite (TTG) affinities

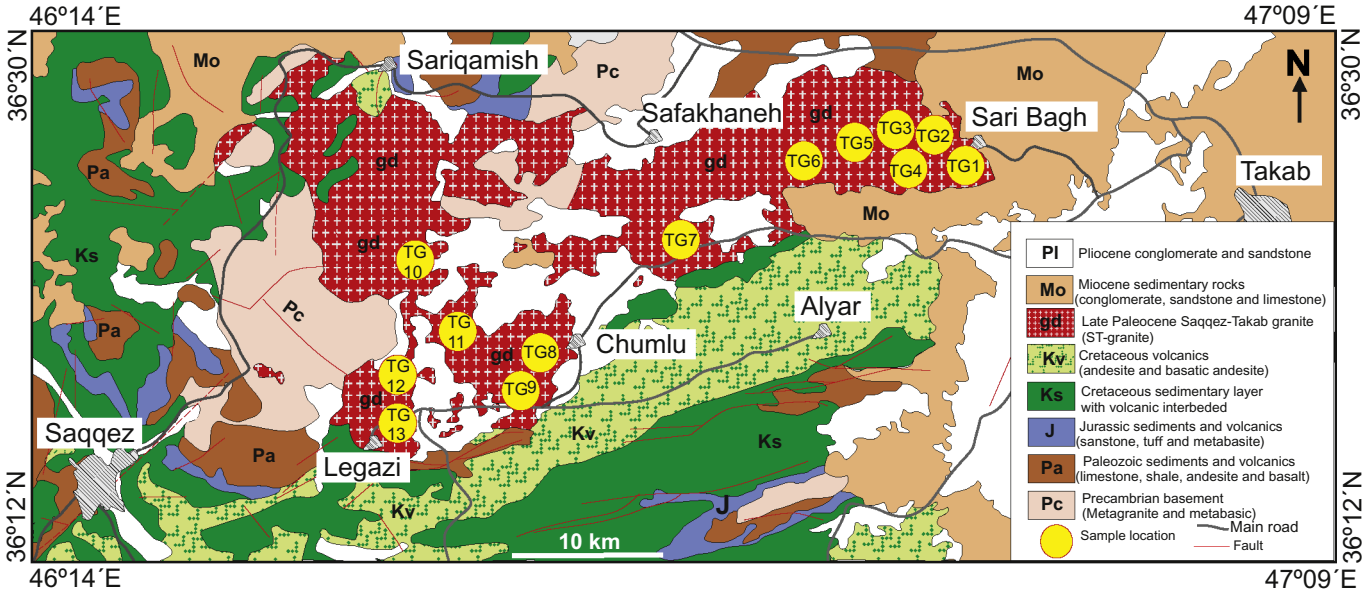

Fig. 2. Simplified geology map of eastern Saqqez (Hariri et al., 2003). ST granite lies between the cities of Saqqez and Takab in northwest Iran. The ST granitoid cuts the Cadomian and Cretaceous rocks and is unconformably overlain by Miocene sedimentary rocks.

have been reported in the Ghalaylan area (Azizi et al., 2015). Eocene to Quaternary adakitic lavas are also present in the Urumieh-Dokhtar magmatic belt (UDMB). Partial melting of Neotethys subducting oceanic crust is suggested for the genesis of Eocene to Quaternary adakites (Ghorbani and Bezenjani, 2011; Omrani, 2018), although other mechanisms such as lower crustal melting under eclogite facies conditions have also been proposed (e.g., Gao et al., 2004). Late Miocene-Pliocene adakitic rocks also occurred in the Hamadan-Tabriz volcanic belt (HTV) of western Iran (Azizi and Moinevaziri, 2009). Jahangiri (2007) considered these as post-collisional adakites that formed as the result of partial melting of oceanic slab in the garnet amphibolite facies. Other mechanisms such as fractionation of hornblende from calc-alkaline magmas was also proposed for the generation of adakites in this belt (Azizi et al., 2014). Late Paleocene-Early Eocene adakitic

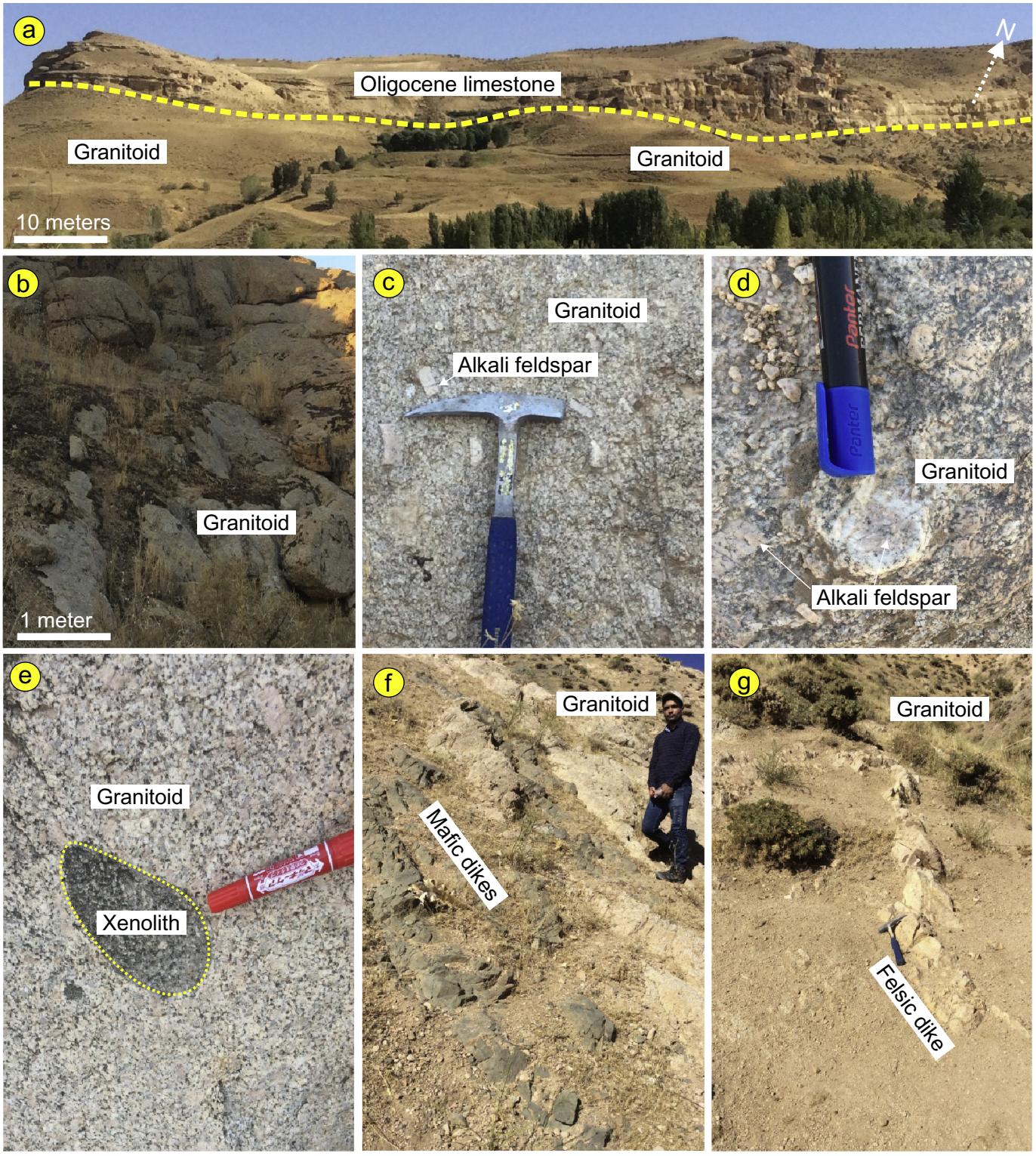

Fig. 3. Field relations of the ST granitoid body. (a) ST granitoid is unconformably overlain by Miocene sedimentary sequences in the eastern part of the Sari Bagh village. (b) Massive structure with cross joints. (c) Alkali feldspar megacrysts in fine-grained granitic matrix. (d) Plagioclase porphyroclast recrystallized due to deformation in foliated granitoid. (e) Rounded mafic enclaves up a few centimeters across. (f-g) Parallel fine-grained mafic and leucogranite dikes which cut the main body.

granitoids associated with intermediate to acidic adakitic volcanic and subvolcanic rocks are also reported from E Turkey, mainly from the eastern Pontides (Fig. 1). Continental thickening and detaching of the lower crust and melting in the hot mantle are the main proposed mechanisms for generating these adakitic magmas (Eyüboglu et al., 2011; Karsli et al., 2010; Topuz et al., 2005, 2011). There are thus different scenarios for generating adakitic magmas in Iran and Eastern Pontides, depending on age and relation to Neotethys closing and Arabia-Eurasia collision.

We build on these insights about adakite magma genesis in investigating Paleocene granitic rocks from NW Iran. We here show that Saqqez-Takab granitoid (hereafter, ST granitoid) differ in age compared to other NW Iran Paleogene granitoids and seems to be a special case. These rocks have similar ages and compositions with adakitic rocks reported in the eastern Pontides. In this work, we focus on new U-Pb zircon ages, whole rock chemistry and Sr-Nd isotope ratios of high K adakitic rocks in NW Iran (Fig. 2) and compare these to similar-aged adakitic rocks in eastern Turkey. We use the compiled dataset to constrain the petrogenesis of these bodies and suggest a new way to generate adakitic melts in regions where the continental crust is only slightly thickened.

1.1. Geological setting and background

Iran is a part of the Alpine-Himalaya orogenic belt, and its basement is dominated by Ediacaran-Early Cambrian (~550 Ma) rocks that formed during the Cadomian orogeny (Shafaii Moghadam and Stern, 2014). The Cadomian basement of Turkey and Iran rifted away from Gondwana and accreted to Eurasia during Triassic time (Stern et al., 2016; Ustaömer et al., 2009). There are several suture zones in Iran, delineating former oceanic basins and continental ribbons of Cadomian crust (Fig. 1). Continental blocks include the Turan block in the NE, NW Iranian and the Central Iranian blocks. The NW Iranian block is separated from the Caucasus by the Sevan-Akera suture zone and from the Arabian platform by the Zagros-Bitlis suture (Fig. 1). Iran is juxtaposed with the Anatolian block in the west and the Afghan block to the east.

There are two other important tectono-magmatic zones in Iran such as the Sanandaj-Sirjan zone (SaSZ) and the Cenozoic Urumieh- Dokhtar magmatic belt (UDMB) (Stöcklin, 1974). The SaSZ is situated between the Zagros fold-thrust belt in the SW and the UDMB in the NE (Stöcklin, 1974). The SaSZ shows evidence of magmatism, metamorphism and deformation from Ediacaran to the Quaternary. Intrusive rocks are abundant in the SaSZ, ranging in age from Ediacaran-Early Cambrian (Hassanzadeh et al., 2008; Shabanian et al., 2018), Carboniferous - Permian (Abdulzahra et al., 2016; Azizi et al., 2017; Bea et al., 2011; Shafaii Moghadam et al., 2015), Jurassic (e.g., Azizi et al., 2011; Deevsalar et al., 2017; Mahmoudi et al., 2011; Shahbazi et al., 2010), and Cretaceous (Abdulzahra et al., 2018) to Paleogene (Deevsalar et al., 2017; Mazhari et al., 2009). There are several geochronological and geochemical studies on the Paleozoic-Mesozoic igneous rocks of the SaSZ, but still the occurrence and geochemical signatures of Paleocene igneous rocks are enigmatic. Paleogene intrusions such as the

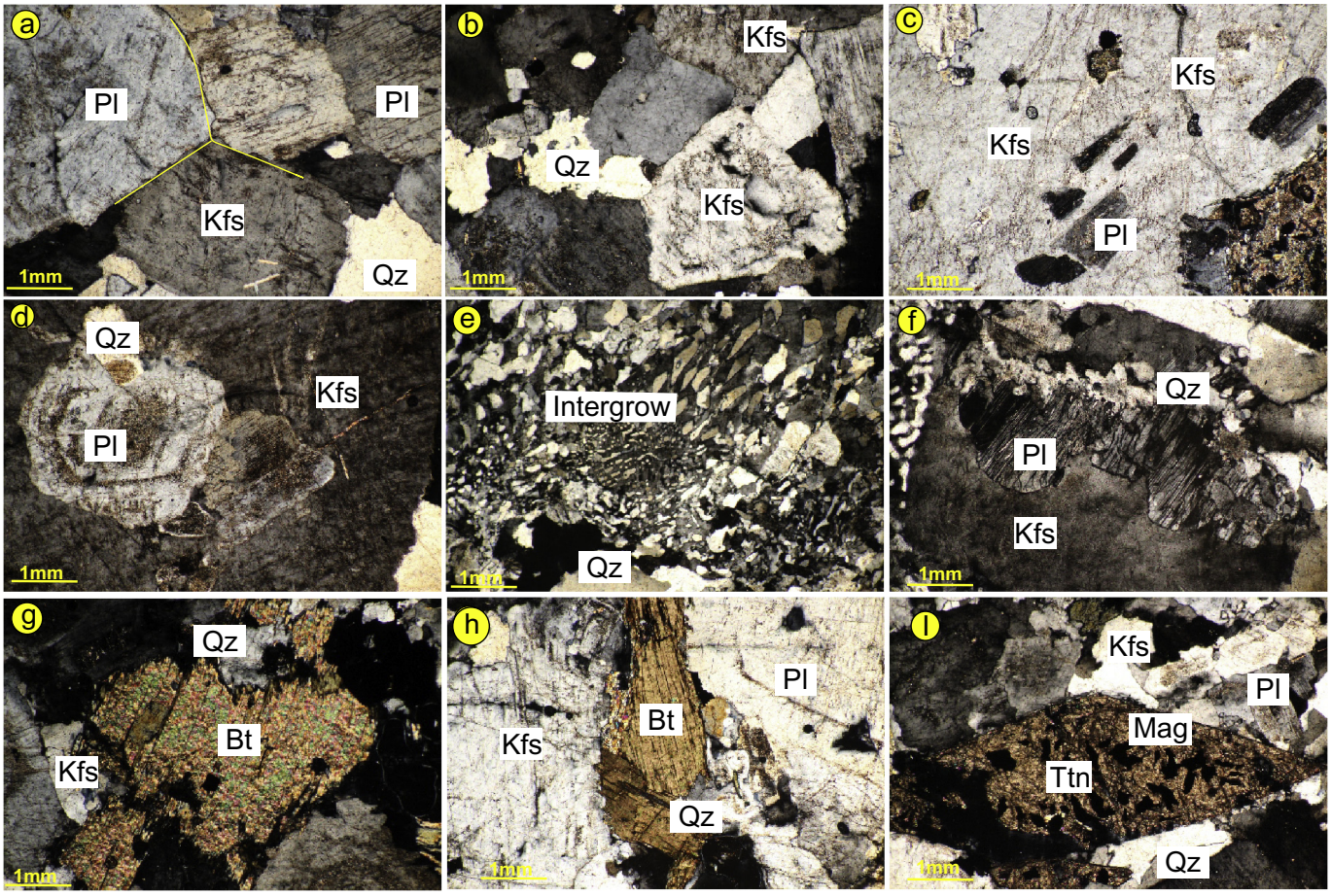

Fig. 4. Photomicrographs of Saqqez-Takab granite in plane-polarized light (PPL). (a-b) Granular texture with equilibrium grain boundaries showing 120° triple junctions. (c-d) K-feldspar is surrounding earlier phases such as plagioclase. (e-f) Intergrown quartz and K-feldspar as graphic texture. (g-h) Biotite which crystallized between alkali feldspar and plagioclase grains in the final stage of magma crystallization. (k) Titanite as minor minerals with lozenge form and magnetite inclusions. *Abbreviations; Hbl = Hornblende, Ttn = Titanite, Mag = Magnetite, Bt = Biotite, Kfs = Alkali feldspar, Pl = Plagioclase, Qz = Quartz* (Abbreviations based on Whitney and Evans, 2010).

ST granitoids are thus important for understanding the Paleogene tectono-magmatic evolution of Iran (Azizi et al., 2019; Mazhari et al., 2011).

1.2. Field relations and petrography

1.2.1. Field relations

The ST granitoids are exposed over an area of ~600 km^2 (~30 km × ~20 km) in the northern SaSZ, between the cities of Saqqez in the west and Takab in the east (Fig. 2). These granitoids were injected into Cadomian igneous rocks and metasedimentary rocks in the north and Cretaceous sedimentary and volcanic rocks in the south and west. The ST granitoids experienced both brittle and ductile deformation in Eocene time as shown by the local cataclastic and mylonitic fabrics. The ST granitoids are unconformably overlain by Oligocene-Miocene sedimentary rocks in the east of Sari Bagh village (Fig. 3a). ST granitoids with massive structure (Fig. 3b), occasionally show porphyroclastic texture represented by oriented alkali-feldspar phenocrysts in a fine-grained matrix (Fig. 3c). Near Saheb city, pink coarse-grained alkali felspars are mantled by white rims (Fig. 3d) in a way similar to rapakivi texture (Fig. 3d). However, rapakivi texture could not been confirmed petrographically. This might be related to the processes of dynamic recrystallization. Rounded mafic enclaves up to a few centimeters across are locally found in the ST granitoids (Fig. 3e). Fine-grained mafic and leucogranite dikes (up to 1 m thick) cutting the main granitoid body are also present (Fig. 3 f-g).

1.3. Petrography

The granitoids are medium to coarse-grained and contain quartz (15–35 vol%), perthitic K-feldspar (20–30 vol%) and plagioclase (30–50 vol%). Accessory minerals are biotite (3–4 vol%), hornblende (2–3 vol%), titanite and titanomagnetite (<1 vol%).The ST granitic rocks vary from quartz monzonite to monzogranite in the quartz-alkali feldspar-plagioclase (QAP) modal classification diagram (Streckeisen, 1974) whereas one mafic dike plots in the monzonite field (Supplementary Fig. A1). The granitoids are medium to coarse-grained and contain quartz (15–35%), perthitic K-feldspar (20–30%) and plagioclase (30–50%). Accessory minerals are biotite (3–4%), hornblende (2–3%), titanite and magnetite (<1%). These granitic rocks have granular texture, with triple junction grain boundaries and some intergrowth textures (Fig. 4a–d). Some K-feldspars megacrysts envelope oriented sodic plagioclase (Fig. 4c) and oscillatory-zoned plagioclase (Fig. 4d). Sometimes, K-feldspars are replaced with altered minerals such as kaolinite and sericite. Intergrowths of quartz and K-feldspar are also common (Fig. 4e). There are some minor myrmekite textures in around some K-feldspars in 1–2 of our samples (Fig. 4f). This is known as rim myrmekite, which is generated in the deformed plutonic rocks (Simpson, 1985). Minor biotite (vol.1–2%; Fig. 4g–h) is fresh and rarely

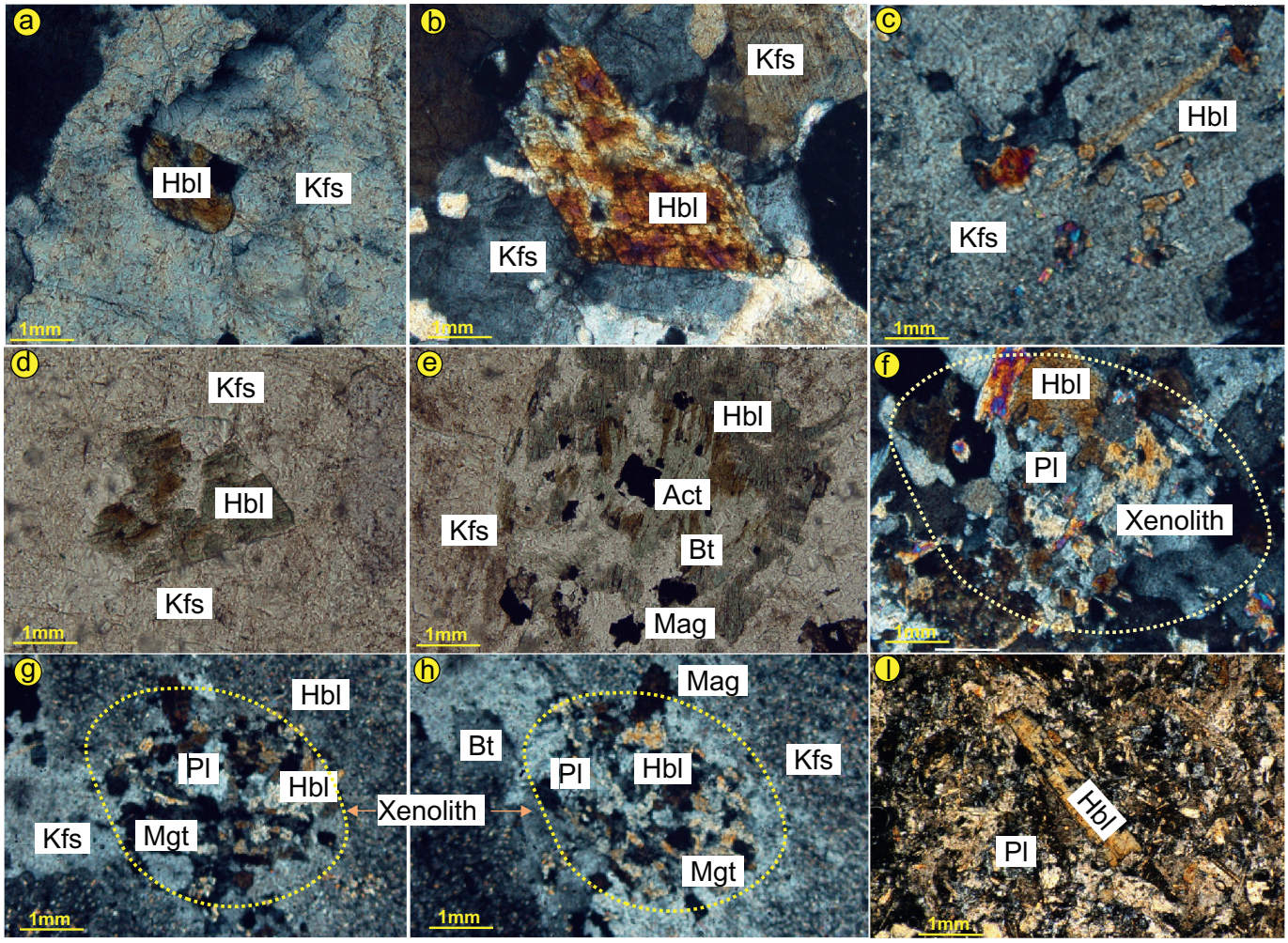

Fig. 5. Photomicrographs of Saqqez-Takab amphiboles and their relationships with other minerals. (a-c) Amphibole grains which are surrounded by alkali felspars grains in cross polarized light (XPL) and plane polarized light (PPL) (d-e). Some amphibole grains were replaced by biotite, actinolite and magnetite (e). Mafic fine-grained xenocrysts which are rich in hornblende, magnetite and feldspars. (i) Mafic dikes with fine-grained porphyritic texture and hornblende phenocrysts. *Abbreviations; Hbl = Hornblende, Act = Actinolite, Mag = Magnetite, Bt = biotite, Kfs = Alkali feldspar, Pl = Plagioclase* (Abbreviation based on Whitney and Evans, 2010).

Table 1
U-Pb isotopic data for zircon grains of Saqqez-Takab (ST) granitoid.

Spot No.	Th/U	^{206}Pbc[a]		$^{207}Pb/^{206}Pb$	Error	$^{206}Pb/^{238}U$	Error	$^{207}Pb/^{235}U$	Error	^{238}U-^{206}Pb	Error	^{235}U-^{207}Pb	Error
		(%)			2σ		2σ		2σ	age(Ma)	2σ	age (Ma)	2σ
TG-9													
TG-9-03	1.13	4.95		0.0139	0.0023	0.0081	0.0003	0.015	0.003	51.9	1.9	15.6	2.6
TG-9-05	0.81	0.76	[b]	0.0603	0.0078	0.0087	0.0003	0.072	0.010	55.7	1.9	70.6	9.5
TG-9-06	1.76	19.07		0.0756	0.0050	0.0096	0.0003	0.100	0.007	61.7	1.9	96.9	7.1
TG-9-07	0.70	8.00		0.0718	0.0060	0.0088	0.0003	0.087	0.008	56.5	1.8	84.9	7.6
TG-9-08	1.28	4.59		0.0282	0.0027	0.0094	0.0003	0.037	0.004	60.6	1.7	36.6	3.6
TG-9-10	1.06	2.15	[b]	0.0377	0.0052	0.0085	0.0003	0.044	0.006	54.3	2.1	43.7	6.3
TG-9-11	0.78	1.93	[b]	0.0529	0.0070	0.0088	0.0004	0.064	0.009	56.2	2.3	62.8	8.7
TG-9-13	1.02	2.06	[b]	0.0446	0.0058	0.0085	0.0003	0.052	0.007	54.6	2.1	51.7	7.0
TG-9-14	1.06	n.d		0.0384	0.0058	0.0114	0.0004	0.061	0.009	73.4	2.7	59.7	9.2
TG-9-15	0.76	0.36	[b]	0.0508	0.0080	0.0088	0.0004	0.061	0.010	56.2	2.3	60.5	9.8
TG-9-16	1.05	3.21		0.0231	0.0033	0.0084	0.0003	0.027	0.004	54.2	2.0	27.0	3.9
TG-9-17	1.04	n.d	[b]	0.0467	0.0063	0.0083	0.0003	0.054	0.007	53.4	1.7	53.0	7.4
TG-9-18	0.75	n.d	[b]	0.0562	0.0093	0.0088	0.0004	0.068	0.012	56.6	2.3	67.2	11.4
TG-9-19	0.66	n.d	[b]	0.0606	0.0114	0.0084	0.0004	0.070	0.014	53.8	2.5	68.7	13.3
TG-9-20	0.81	4.13		0.0161	0.0023	0.0085	0.0003	0.019	0.003	54.3	1.9	18.9	2.8
TG-9-21	0.65	1.17		0.0509	0.0069	0.0092	0.0003	0.065	0.009	59.3	2.1	63.8	8.9
TG-9-22	0.68	8.27		0.0803	0.0080	0.0087	0.0003	0.097	0.010	56.1	2.2	93.9	10.0
TG-9-23	1.22	1.43		0.0296	0.0040	0.0084	0.0003	0.034	0.005	53.7	1.6	34.1	4.7
TG-9-24	0.73	2.80		0.0319	0.0049	0.0081	0.0003	0.036	0.006	51.9	2.0	35.4	5.6
TG-9-25	0.93	1.61	[b]	0.0356	0.0050	0.0088	0.0003	0.043	0.006	56.2	1.9	42.8	6.2
TG-9-26	0.73	n.d	[b]	0.0419	0.0082	0.0087	0.0004	0.050	0.010	55.8	2.3	49.7	10.0
TG-9-28	1.97	0.21	[b]	0.0442	0.0059	0.0086	0.0003	0.052	0.007	55.3	1.8	51.9	7.2
TG-9-29	0.66	1.64	[b]	0.0494	0.0078	0.0080	0.0003	0.055	0.009	51.6	2.1	54.1	8.8
TG-9-30	0.89	2.38		0.0297	0.0051	0.0084	0.0003	0.034	0.006	53.8	2.1	34.3	6.0
TG-9-31	0.71	5.08		0.0082	0.0017	0.0081	0.0004	0.009	0.002	52.0	2.4	9.3	2.0
TG-9-32	0.72	n.d	[b]	0.0548	0.0087	0.0085	0.0003	0.064	0.010	54.3	2.1	62.9	10.3
TG-9-34	0.92	n.d	[b]	0.0605	0.0083	0.0082	0.0003	0.069	0.010	52.8	1.7	67.4	9.5
TG-9-36	0.91	n.d		0.1313	0.0136	0.0085	0.0003	0.154	0.017	54.5	2.0	145.2	16.0
TG-9-37	0.75	5.41		0.0139	0.0023	0.0081	0.0003	0.016	0.003	52.2	2.0	15.7	2.7
TG-9-38	0.86	0.02	[b]	0.0667	0.0092	0.0083	0.0003	0.076	0.011	53.3	1.8	74.7	10.7
TG-9-39	0.85	4.82		0.0166	0.0026	0.0085	0.0003	0.019	0.003	54.4	2.0	19.5	3.2
TG-9-40	0.85	n.d	[b]	0.0578	0.0090	0.0087	0.0003	0.069	0.011	55.7	2.0	67.8	10.8
TG-9-41	0.84	0.63	[b]	0.0458	0.0101	0.0094	0.0004	0.059	0.013	60.4	2.7	58.6	13.2
TG-9-42	0.84	n.d	[b]	0.0462	0.0082	0.0092	0.0003	0.059	0.011	59.0	2.2	57.9	10.4
TG-9-43	1.35	n.d	[b]	0.0527	0.0081	0.0091	0.0003	0.066	0.010	58.2	2.1	64.8	10.3
TG-9-45	0.91	3.90		0.0165	0.0028	0.0090	0.0003	0.020	0.004	57.7	2.2	20.6	3.6
TG-9-46	0.80	n.d	[b]	0.0530	0.0094	0.0097	0.0004	0.071	0.013	62.5	2.5	69.7	12.7
TG-9-47	1.47	1.72	[b]	0.0393	0.0046	0.0096	0.0003	0.052	0.006	61.7	1.9	51.6	6.2
TG-9-49	2.99	13.01		0.0417	0.0020	0.0103	0.0002	0.059	0.003	66.0	1.3	58.3	3.0
TG-9-50	1.08	n.d	[b]	0.0509	0.0073	0.0090	0.0003	0.063	0.009	57.8	1.9	62.2	9.2
TG-9-51	0.75	4.37		0.0110	0.0021	0.0090	0.0004	0.014	0.003	57.5	2.3	13.6	2.7
TG-9-52	1.27	n.d	[b]	0.0490	0.0065	0.0088	0.0003	0.059	0.008	56.5	1.7	58.6	8.0
TG-9-53	0.84	n.d	[b]	0.0651	0.0097	0.0091	0.0003	0.081	0.012	58.2	2.2	79.5	12.2
TG-9-54	1.02	4.29		0.0171	0.0021	0.0084	0.0002	0.020	0.002	54.0	1.6	20.0	2.5
TG-9-55	1.06	n.d	[b]	0.0605	0.0083	0.0088	0.0003	0.074	0.010	56.8	1.9	72.3	10.2
TG-9-56	0.69	n.d	[b]	0.0574	0.0097	0.0094	0.0004	0.074	0.013	60.3	2.4	72.8	12.6
TG-9-58	1.02	0.72	[b]	0.0491	0.0070	0.0089	0.0003	0.061	0.009	57.4	2.0	59.7	8.8
TG-9-60	1.09	n.d	[b]	0.0464	0.0119	0.0090	0.0004	0.057	0.015	57.5	2.8	56.7	14.7
TG-9-61	0.87	n.d	[b]	0.0420	0.0078	0.0092	0.0003	0.053	0.010	59.2	2.2	52.8	10.0
TG-9-62	0.74	n.d	[b]	0.0474	0.0099	0.0096	0.0004	0.063	0.013	61.5	2.6	61.7	13.1
TG-9-63	0.55	n.d	[b]	0.0482	0.0112	0.0089	0.0004	0.059	0.014	56.9	2.6	58.1	13.7
TG-9-64	0.84	n.d	[b]	0.0467	0.0081	0.0092	0.0003	0.059	0.011	58.9	2.2	58.3	10.4
TG-11													
TG-11-01	0.65	n.d	[b]	0.0480	0.0097	0.0086	0.0003	0.057	0.012	55.2	2.2	56.2	11.6
TG-11-02	0.76	0.82		0.0465	0.0049	0.0165	0.0004	0.106	0.011	105.6	2.8	102.2	11.0
TG-11-03	0.68	0.68	[b]	0.0389	0.0052	0.0084	0.0002	0.045	0.006	54.2	1.6	44.9	6.1
TG-11-04	1.61	n.d	[b]	0.0488	0.0053	0.0094	0.0002	0.063	0.007	60.4	1.6	62.4	6.9
TG-11-05	0.97	4.58	[b]	0.0324	0.0043	0.0086	0.0003	0.038	0.005	55.3	1.9	38.4	5.3
TG-11-06	0.74	1.29	[b]	0.0348	0.0070	0.0088	0.0003	0.042	0.009	56.4	2.2	41.9	8.6
TG-11-07	0.93	0.09	[b]	0.0531	0.0080	0.0087	0.0003	0.064	0.010	56.0	1.9	62.9	9.8
TG-11-08	0.72	n.d	[b]	0.0533	0.0099	0.0091	0.0004	0.067	0.013	58.5	2.3	65.8	12.5
TG-11-10	1.50	n.d	[b]	0.0564	0.0069	0.0091	0.0003	0.071	0.009	58.6	2.0	69.7	8.9
TG-11-11	0.84	2.41	[b]	0.0278	0.0044	0.0086	0.0003	0.033	0.005	55.3	2.1	33.0	5.3
TG-11-12	0.82	0.54	[b]	0.0379	0.0065	0.0090	0.0003	0.047	0.008	57.5	2.2	46.4	8.1
TG-11-13	0.59	n.d	[b]	0.0534	0.0100	0.0094	0.0004	0.069	0.013	60.1	2.7	67.7	13.0
TG-11-14	0.85	3.77	[b]	0.0104	0.0016	0.0085	0.0003	0.012	0.002	54.4	2.0	12.2	2.0
TG-11-15	0.84	n.d		0.0584	0.0108	0.0091	0.0004	0.073	0.014	58.4	2.7	71.8	13.7
TG-11-16	0.79	6.50		0.0163	0.0020	0.0081	0.0003	0.018	0.002	51.9	1.9	18.3	2.3
TG-11-17	2.60	n.d	[b]	0.0511	0.0073	0.0087	0.0003	0.061	0.009	55.9	1.7	60.5	8.9
TG-11-18	1.11	n.d	[b]	0.0439	0.0068	0.0090	0.0003	0.055	0.009	57.8	1.8	54.0	8.5
TG-11-19	0.68	4.00		0.0333	0.0056	0.0086	0.0003	0.040	0.007	55.4	2.2	39.5	6.8
TG-11-20	0.70	6.58	[b]	0.0011	0.0002	0.0079	0.0003	0.001	0.000	51.0	2.0	1.3	0.2

Table 1 (*continued*)

Spot No.	Th/U	^{206}Pbc[a] (%)		$^{207}Pb/^{206}Pb$	Error 2σ	$^{206}Pb/^{238}U$	Error 2σ	$^{207}Pb/^{235}U$	Error 2σ	^{238}U-^{206}Pb age(Ma)	Error 2σ	^{235}U-^{207}Pb age (Ma)	Error 2σ
TG-11-21	0.94	5.13	[b]	0.0091	0.0014	0.0085	0.0003	0.011	0.002	54.6	1.8	10.8	1.7
TG-11-22	0.72	1.50	[b]	0.0235	0.0055	0.0092	0.0004	0.030	0.007	58.9	2.3	29.7	7.1
TG-11-23	1.08	n.d	[b]	0.0476	0.0056	0.0086	0.0002	0.056	0.007	55.2	1.4	55.8	6.8
TG-11–24	0.70	n.d	[b]	0.0419	0.0090	0.0087	0.0003	0.050	0.011	55.5	2.1	49.6	10.8
TG-11-26	1.05	1.04	[b]	0.0334	0.0043	0.0100	0.0003	0.046	0.006	64.1	2.0	45.6	6.0
TG-11-27	0.53	n.d	[b]	0.0486	0.0107	0.0089	0.0004	0.060	0.013	57.4	2.7	59.0	13.3
TG-11-28	0.77	n.d	[b]	0.0497	0.0133	0.0087	0.0005	0.060	0.016	55.8	3.0	58.7	16.0
TG-11-29	0.70	n.d	[b]	0.0409	0.0083	0.0086	0.0004	0.048	0.010	55.0	2.3	47.9	9.9
TG-11-30	0.69	6.01	[b]	0.0018	0.0004	0.0084	0.0004	0.002	0.000	53.6	2.4	2.2	0.4
TG-11-31	0.89	n.d	[b]	0.0530	0.0080	0.0088	0.0003	0.065	0.010	56.6	2.1	63.5	9.8
TG-11-32	1.12	n.d		0.0464	0.0069	0.0106	0.0004	0.068	0.010	67.9	2.4	66.5	10.2
TG-11-33	0.78	1.67	[b]	0.0324	0.0056	0.0084	0.0003	0.038	0.007	54.1	2.1	37.5	6.6
TG-11-34	0.71	3.85	[b]	0.0107	0.0020	0.0084	0.0003	0.012	0.002	53.9	2.2	12.5	2.4
TG-11–35	0.74	2.80	[b]	0.0238	0.0041	0.0089	0.0003	0.029	0.005	56.8	2.2	29.1	5.1
TG-11-36	2.90	3.62		0.0448	0.0047	0.0081	0.0003	0.050	0.005	52.1	1.7	49.6	5.4
TG-11-37	0.97	2.57		0.0348	0.0043	0.0093	0.0003	0.045	0.006	59.8	2.0	44.4	5.7
TG-11-38	0.93	5.84		0.0062	0.0017	0.0094	0.0006	0.008	0.002	60.2	3.5	8.1	2.3
TG-11-39	1.13	n.d	[b]	0.0521	0.0092	0.0095	0.0004	0.069	0.012	61.2	2.5	67.3	12.2
TG-11-40	0.71	1.23		0.0356	0.0058	0.0108	0.0004	0.053	0.009	69.5	2.6	52.7	8.8
TG-11-41	0.80	n.d	[b]	0.0472	0.0069	0.0096	0.0003	0.063	0.009	61.9	2.0	61.8	9.2
TG-11-42	0.88	3.79	[b]	0.0182	0.0034	0.0094	0.0004	0.024	0.004	60.1	2.4	23.6	4.5
TG-11-43	0.90	2.93	[b]	0.0160	0.0032	0.0092	0.0004	0.020	0.004	59.3	2.3	20.5	4.2
TG-11-44	0.85	0.18	[b]	0.0454	0.0083	0.0093	0.0004	0.058	0.011	59.5	2.3	57.4	10.7
TG-11-45	0.79	n.d	[b]	0.0567	0.0093	0.0093	0.0004	0.073	0.012	59.8	2.3	71.4	12.1
TG-11-47	0.75	n.d	[b]	0.0490	0.0089	0.0094	0.0004	0.063	0.012	60.1	2.3	62.3	11.6

[a] Percentage of ^{206}Pb contributed by common Pb on the basis of ^{204}Pb. Value of common Pb was assumed by Stacey and Kramer (1975) model; n.d.: no detection of ^{204}Pb.
[b] Selected for age calculation.

replaced by chlorite and magnetite in the rim. Biotite is interstitial between alkali feldspar and plagioclase (Fig. 4h). Lozenge-shaped titanite with magnetite (titanomagnetite) inclusions are the main accessory mineral (Fig. 4i). Euhedral hornblende is found as inclusions in alkali feldspars (Fig. 5a–e) and in some grains is replaced by biotite, actinolite and magnetite (Fig. 5e). Petrographic observations indicate that the crystallization sequence was plagioclase, hornblende, K-feldspar, biotite and quartz.

Minor micro-dioritic xenoliths are fine-grained and consist of feldspars and hornblende (Fig. 5 f–h). Mafic dikes are fine-grained, porphyritic and highly altered (Fig. 5i). Amphibole phenocrysts are set in a highly altered groundmass of amphibole, K- feldspar and plagioclase. Plagioclase microlites which dominate the groundmass are replaced by albite, calcite and sericite dominate the groundmass.

1.4. Methods and techniques

We used multiple techniques in this study. Cathodoluminescence (CL) and back-scatter electron (BSE) techniques were used to image zircons. U-Pb zircon ages were determined by laser ablation – inductively coupled mass spectrometry (LA-ICP-MS). Whole rock major element compositions were determined by wavelength dispersive X-ray fluorescence (XRF). Trace elements were determined by ICP-MS. Whole-rock Sr and Nd isotopic ratios were determined by thermal ionization mass spectrometry. Analytical details are presented in Supplementary Document DR.1. Nd model ages were calculated using $T_{DM} = 1/\lambda$ *ln [($^{143}Nd/^{144}Nd_{sample}$-0. 512,638)/($^{147}Sm/^{144}Nd_{sample}$-0.2137) + 1] algorithm (Jahn et al., 1999).

2. Results

2.1. U-Pb Zircon ages

To constrain the igneous crystallization age of the Saqqez-Takab pluton, zircons were separated from two fresh samples (TG-9 and TG-11). CL and BSE images for zircons from both samples show prismatic shapes with fine oscillatory zoning (Supplementary Fig. A2) Some internal structures suggest inherited cores, but analyses yield the same ages for cores and rims (Supplementary Fig. A2). Most zircons have Th/U ratios <1 (Table 1), rarely up to 3, demonstrating that these are magmatic.

Zircons from sample TG-9 reveal a Concordia age of 57.8 ± 0.9 Ma (2σ error) and a mean weighted ^{238}U-^{206}Pb age of 57.5 ± 0.7 Ma (2σ error). Sample TG-11 zircons show a Concordia age of 57.0 ± 1.4 Ma (2σ error), whereas its mean weighted ^{238}U-^{206}Pb age is 56.4 ± 0.8 Ma (Fig. 6a–f). These ages indicate that the ST intrusion crystallized at 57.8 ± 0.9 and 56.4 ± 0.8 Ma (2σ error), in Late Paleocene time (Thanetian).

2.2. Whole rock chemistry

Major and trace element chemical compositions of twelve ST granitoid samples and one mafic dike are listed in Table 2. The ST granitoid is characterized by high contents of SiO_2 (67.3–78.6 wt%), Na_2O (3.9–5.3 wt%) and K_2O (2.2–4.9 wt%), and low contents of TiO_2 (<1.0 wt%), MgO (<2.3 wt%) and CaO (<3.24 wt%). The ST granitoids show also some similarities to sanukitoids (e.g., porphyritic plutonic rocks with alkali feldspar megacrysts and high K_2O contents). The term "sanukitoid" was first used for some Archean high-K TTG rocks (Stern et al., 1989). It was originally defined by Stern et al. (1989) to refer to plutonic rocks containing 55–60 wt% SiO_2, with Mg# >0.6, Ni >100 ppm, Cr >200 ppm, K_2O > 1 wt%, Rb/Sr <0.1, Ba >500 ppm, Sr >500 ppm, enrichment in LREEs, and no or minor negative to positive Eu anomalies. Sanukitoids are broadly related to Cenozoic adakites. ST granitoids are similar to sanukitoids in terms of Ba and Sr contents but contain more SiO_2 (66–72 wt%) and less MgO (<1.2 wt%), Ni (<30 ppm) and Cr (<50 ppm); therefore, the ST granitoids mostly resemble K-rich adakitic rocks rather than sanukitoids.

As noted earlier, Late Paleocene to Early Eocene adakites are widespread in the eastern Pontides of NE Turkey (Karsli et al., 2010; Eyüboglu et al., 2011; Topuz et al., 2005, 2011). These adakitic rocks are contemporaneous with the ST granitoid and are

located far from the Zagros-Bitlis suture zone. Comparing the chemical and isotopic compositions of these rocks with the ST granitoids is useful for understanding the origin of Late Paleocene-Early Eocene adakites in the larger NW Iran- NE Turkey region (Karsli et al., 2010; Eyüboglu et al., 2011; Topuz et al., 2005, 2011). Therefore, we plotted all of the late Paleocene adakites in both Turkey along with the ST granitoids. In NW Iran there are no other reports of Paleocene adakitic rocks.

Based on the variation of silica versus $Na_2O + K_2O$ (Middlemost, 1994), the ST samples plot in fields for quartz-monzonite to granite (Fig. 7a) and the mafic dike plots in the monzogabbro (monzodiorite) domain; these classifications are consistent with the QAP

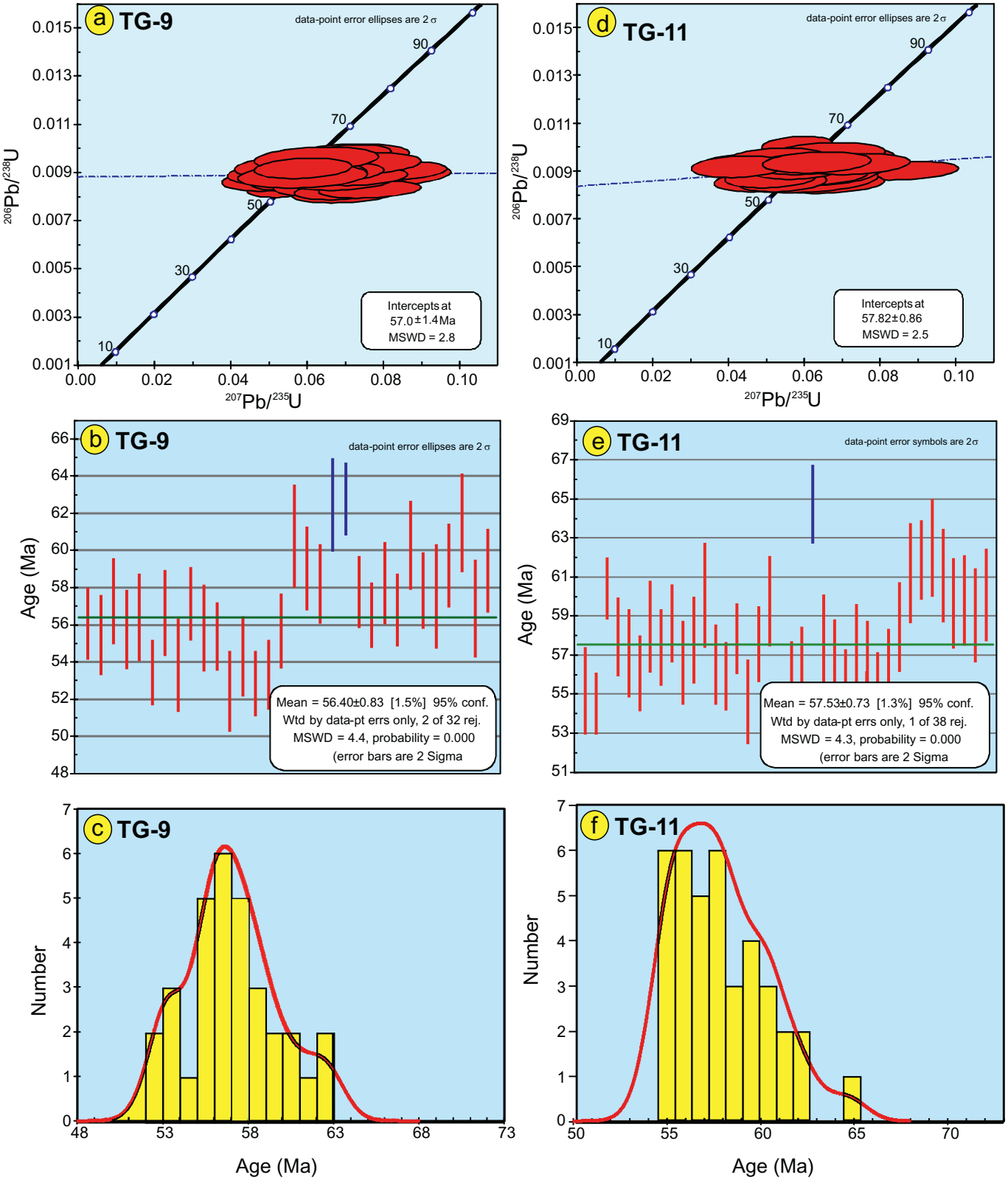

Fig. 6. Concordia diagrams, ^{238}U-^{206}Pb average ages and histograms of zircon ages for TG-9 (a-c) and TG-11 (d-f).

Table 2
Chemical compositions of the ST granitoid and mafic dike.

Sample	TG-1	TG-2	TG-3	TG-4	TG-5	TG-6	TG-7	TG-8	TG-9	TG-10	TG-11	TG-12	TG-13
Rock type	Adakite	Adakite	Adakite	Adakite	Mafic dike	Adakite	Adakite	Adakite	Adakite	Adakite	Adakite	Adakite	Adakite
SiO_2 (wt%)	70.9	67.3	75.7	78.6	51.5	59.1	68.5	70.2	69.4	69.6	66.4	70.3	62.0
TiO_2	0.05	0.40	0.22	0.04	1.05	0.86	0.36	0.36	0.31	0.35	0.34	0.34	0.93
Al_2O_3	15.6	15.2	14.5	13.4	15.1	15.4	16.9	15.3	15.0	16.2	15.7	15.0	15.6
$Fe_2O_3^t$	0.884	2.56	1.97	0.88	7.33	5.22	2.82	2.43	2.48	2.42	2.38	2.54	4.42
MnO	0.001	0.028	0.017	0.002	0.121	0.080	0.028	0.035	0.033	0.030	0.032	0.027	0.055
MgO	0.091	1.15	0.48	0.10	7.07	4.15	1.15	1.20	1.07	1.10	1.05	1.00	2.14
CaO	1.93	2.21	0.98	0.58	6.50	4.54	2.19	2.24	1.99	2.13	1.81	2.26	3.24
Na_2O	4.76	4.74	4.17	3.96	3.95	4.42	4.33	5.04	4.70	5.24	4.47	5.14	4.78
K_2O	3.68	3.14	4.14	4.52	2.32	2.25	4.82	3.37	3.29	3.06	4.93	2.68	4.32
P_2O_5	0.02	0.18	0.08	0.01	0.41	0.34	0.18	0.18	0.16	0.16	0.14	0.15	0.40
LOI	0.61	0.85	0.67	0.29	3.21	2.42	1.26	1.36	0.70	0.98	0.68	0.53	1.21
Total	98.5	97.8	102.9	102.3	98.5	98.8	102.5	101.7	99.1	101.2	97.9	100.0	99.0
Sc (ppm)	0.982	3.08	1.22	0.216	18.9	10.8	3.01	2.98	2.97	2.78	2.97	3.12	6.23
V	8.65	35.2	20.8	4.78	144	86.9	32.8	31.7	28.2	27.2	28.7	28.3	75.8
Cr	7.66	17.0	8.12	4.57	297	139	23.9	19.5	18.9	18.2	31.3	18.1	38.8
Co	0.665	5.60	2.73	0.649	28.5	17.9	4.80	5.27	4.86	4.64	4.87	4.75	11.9
Ni	5.00	14.6	8.04	6.52	138	126	21.1	23.8	13.8	23.8	27.9	55.0	30.7
Cu	8.73	6.93	11.9	7.95	40.2	27.9	12.5	8.95	7.36	7.32	7.65	7.56	28.0
Zn	5.60	25.6	26.8	11.3	95.8	79.6	23.8	39.3	34.0	34.7	36.2	31.5	52.4
Ga	16.2	18.5	16.4	16.1	19.4	20.0	17.5	18.1	18.1	19.3	18.2	19.4	20.4
Rb	61.0	55.9	68.8	122	72.3	70.5	88.9	83.5	77.1	82.4	95.7	79.9	123
Sr	687	939	520	237	837	760	1020	644	842	783	956	838	928
Zr	10.9	8.78	22.6	9.04	198	198	15.2	10.4	9.93	13.4	14.4	12.8	19.7
Nb	6.38	21.2	15.3	4.93	18.4	15.1	19.5	17.1	14.2	17.2	18.7	16.7	53.5
Cs	0.896	0.925	0.636	1.67	0.867	0.570	1.05	1.44	1.72	3.64	1.79	3.55	3.34
Ba	1207	1138	786	178	800	843	2188	887	779	793	2466	569	949
Pb	8.02	13.2	22.2	16.5	28.3	18.2	15.4	15.6	14.0	13.9	17.6	14.8	13.7
Th	5.61	15.3	17.2	9.60	8.59	9.29	13.5	15.5	12.9	12.9	12.6	11.9	27.2
U	0.376	1.87	1.56	2.30	2.98	2.80	2.21	3.00	1.68	3.45	1.59	1.67	6.83
Hf	0.420	0.487	0.916	0.694	5.19	5.08	0.655	0.532	0.508	0.789	0.624	0.737	1.24
Ta	0.495	1.26	0.913	0.335	0.969	0.777	1.08	0.864	0.713	0.899	1.07	0.842	2.94
Y	1.40	5.06	3.47	0.265	16.7	10.5	4.71	4.17	3.43	3.94	5.24	4.21	10.9
La (ppm)	11.2	42.2	29.5	12.5	45.2	42.0	35.1	34.4	27.9	32.3	34.0	32.0	70.4
Ce	15.1	61.7	41.4	7.91	86.2	74.7	55.7	51.5	43.5	48.4	55.8	48.1	122
Pr	1.27	5.76	3.71	0.377	9.77	7.88	5.38	4.76	4.03	4.48	5.42	4.48	12.1
Nd	3.82	19.1	12.0	0.847	36.6	28.6	17.9	16.0	13.3	14.5	18.3	14.8	40.7
Sm	0.413	2.60	1.57	0.071	5.99	4.32	2.16	2.07	1.70	1.84	2.29	1.95	5.34
Eu	0.249	0.780	0.451	0.064	1.71	1.30	0.706	0.658	0.586	0.623	0.722	0.628	1.33
Gd	0.389	1.82	1.11	0.057	4.68	3.23	1.73	1.47	1.27	1.43	1.79	1.38	3.89
Tb	0.046	0.206	0.121	nd	0.597	0.411	0.196	0.167	0.132	0.171	0.197	0.166	0.455
Dy	0.325	1.04	0.683	0.044	3.43	2.25	1.02	0.829	0.727	0.843	1.07	0.798	2.30
Ho	0.059	0.185	0.118	0.007	0.642	0.391	0.175	0.148	0.115	0.132	0.177	0.143	0.421
Er	0.153	0.481	0.327	0.033	1.76	1.07	0.465	0.405	0.352	0.383	0.498	0.414	1.02
Tm	0.024	0.067	0.048	0.005	0.247	0.153	0.069	0.054	0.049	0.052	0.065	0.056	0.154
Yb	0.180	0.420	0.300	0.036	1.54	1.03	0.400	0.348	0.285	0.342	0.423	0.360	0.922
Lu	0.029	0.052	0.049	0.007	0.227	0.143	0.064	0.052	0.043	0.046	0.049	0.057	0.143
Sr/Y	490	186	150	894	50.2	72.6	217	154	245	199	183	199	85.5
La/Yb	62.6	100.4	98.2	350	29.3	40.7	87.8	98.8	98.1	94.4	80.2	88.9	76.3
Ba/Th	215	74.5	45.7	18.6	93.1	90.8	162	57.4	60.3	61.7	195	47.6	34.8
Nb/La	0.567	0.504	0.518	0.394	0.407	0.360	0.555	0.497	0.508	0.534	0.550	0.522	0.761
Mg#	0.17	0.47	0.33	0.19	0.66	0.61	0.45	0.50	0.46	0.48	0.47	0.44	0.49

nd = not determined.
Mg# = [MgO]/([MgO]+[FeO]).
FeO ≈ 0.899*$Fe_2O_3^t$.

modal classification. In the K_2O-SiO_2 bivariant diagram (Peccerillo and Taylor, 1976) the ST granitoids plot in the high-K calc-alkaline to shoshonitic series (Fig. 7b). In the Anorthite-Orthoclase-Albite normative triangle diagram (O'connor, 1965), NE Turkey adakites mainly plot in tonalite and ST granitoids plot in the granitoid fields (Fig. 7c). CIPW norm calculation results are listed in Supplementary Table A1.

Trace element and REE data are summarized in Fig. 8a and b. Compared with primitive mantle (Sun and McDonough, 1989), the ST granitoids are strongly enriched in large ion lithophile elements (LILEs) such as Rb, Ba, K, Pb, and Sr and strongly depleted in high field strength elements (HFSEs) such as Nb, Ta and Zr. The mafic dike is geochemically similar to the granitoids except for lacking a negative Zr anomaly and higher contents of HREEs (Fig. 8b), Cr (297 ppm), Co (28.5 ppm), Fe_2O_3 (7.33 wt%), CaO and MgO (7.07 and 6.50 wt%, respectively). Chondrite-normalized REE patterns for ST granitoids are very similar with negative slopes from LREEs to $HREE_S$, without any Eu anomaly (Fig. 8b). High Ba content, low Rb/Sr ratio and high ratios of Sr/Y and La/Yb are characteristics of ST granitoids. The granitoids plot in the adakite field in the Sr/Y vs Y and La/Yb vs Yb diagrams (Fig. 9a, b) and resemble typical adakites as defined by Defant and Drummond (1990).

2.3. Sr-Nd isotope ratios

The Sr and Nd isotope ratios of twelve ST granitoids and one mafic dike are listed in Table 3. The samples have moderately low $^{87}Rb/^{86}Sr$

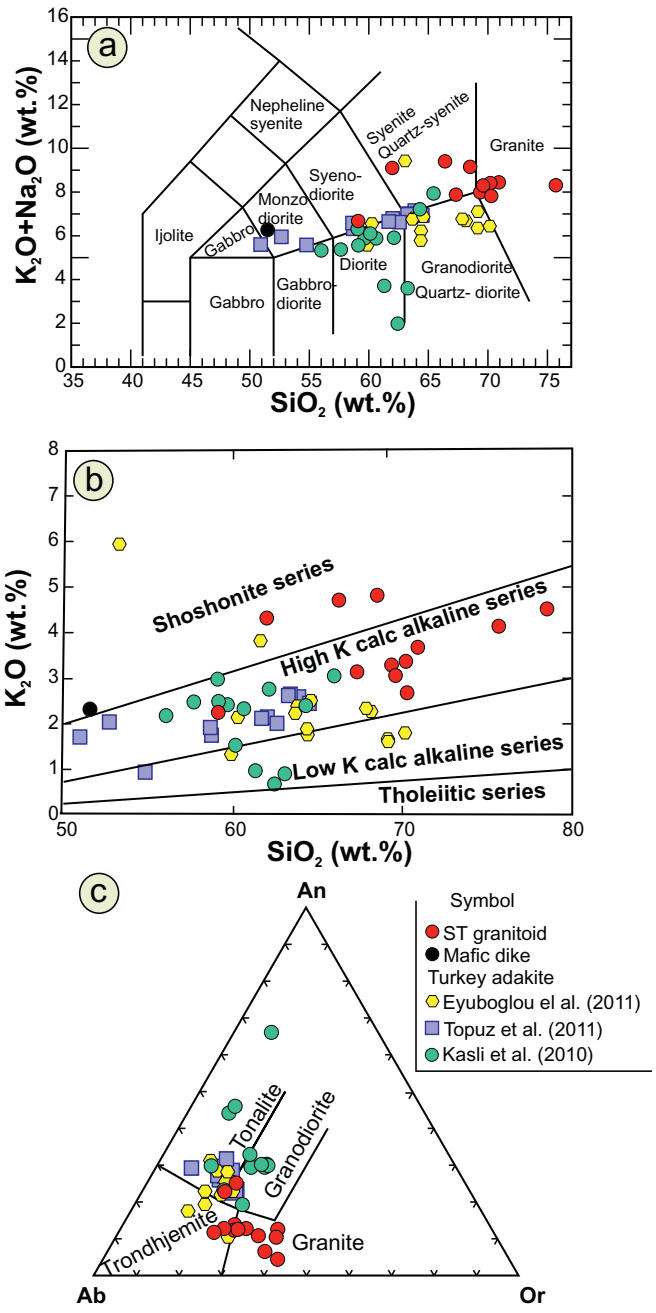

Fig. 7. (a) Variation of $Na_2O + K_2O$ vs. SiO_2 (Middlemost, 1994). ST samples plot in the quartz-monzonite and granite fields and mafic dikes plot in the monzodiorite field. (b) K_2O-SiO_2 diagram showing that ST granitoids and Turkey adakites plot as high-K calc alkaline to shoshonitic series. (c) Anorthite-orthoclase-albite normative diagram (O'connor, 1965). Eastern Turkey adakite and ST granitoids mainly plot in the tonalite and granitoid fields respectively.

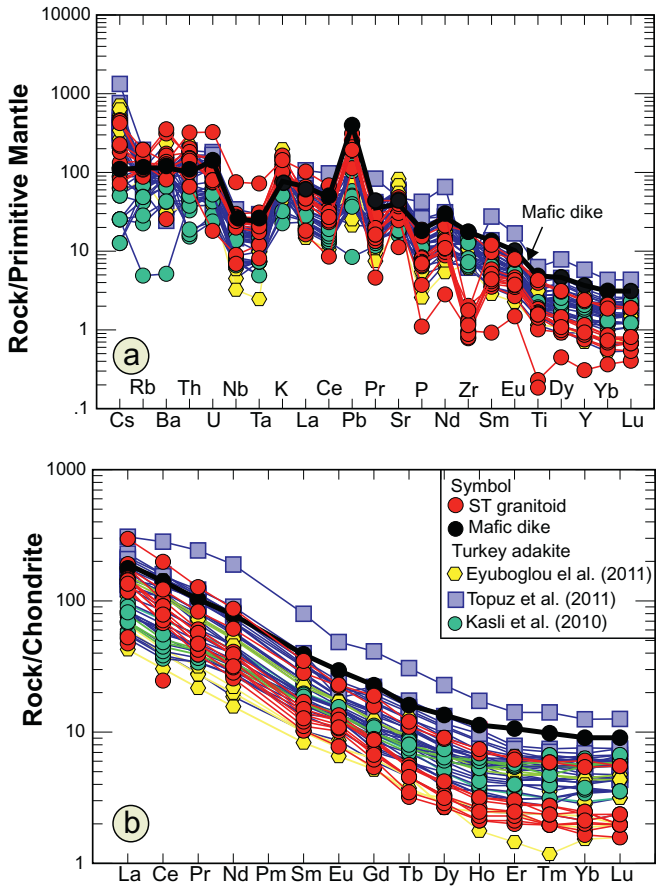

Fig. 8. (a) Trace elements normalized to primitive mantle and (b) Chondrite-normalized REE patterns (Sun and McDonough, 1989) showing similarities for adakites in NW Iran and NE Turkey. Negative Nb and Ta anomalies and absence of Eu negative anomalies are observed for all samples. The absence of Lu and Yb depletions argue against an important role for garnet in the sources of these rocks.

(0.25–1.49; mean = 0.38) so the initial ratios of $^{87}Sr/^{86}Sr$ are likely to be meaningful. Initial $^{87}Sr/^{86}Sr$ and $^{143}Nd/^{144}Nd$ ratios were calculated based on U-Pb zircon ages. The initial ratio of $^{87}Sr/^{86}Sr(i)$ in ST granitoids varies from 0.7044 to 0.7053, and their $\varepsilon_{Nd}(t)$ value varies from −2.8 and + 2.0; most samples are slightly positive (+0.3 to +0.7). The mafic dike differs slightly from the ST granitoid, with $^{87}Sr/^{86}Sr(i)$ = 0.7054 and slightly negative $\varepsilon_{Nd}(t)$ (−1.4). $^{147}Sm/^{144}Nd$ are low (0.05–0.10; mean = 0.08) so T_{DM} model ages are useful to calculate. These show ST granitoid model ages are around 0.46 to 0.70 Ga, consistent with derivation from Cadomian lithospheric mantle and/or crust. The mafic dike has a slightly older T_{DM} (0.79Ga) indicating some differences with ST granitoid.

3. Discussion

Below we use our new data to address several questions: 1) What was the source of ST granitic magmas? 2) How did these magmas evolve? and 3) what do ST adakitic granitoid rocks of NW Iran and eastern Pontides (Turkey) tell us about the geodynamic evolution of this region in early Paleogene time?

3.1. Source region of magma

The geochemical signatures of the ST granitoids such as high Sr/Y, La/Yb and LREEs/HREEs ratios confirm their similarities to typical adakites. Negative Nb and Ta anomalies along with low Y, Sc and HREE abundances may have been controlled by garnet, hornblende and rutile (± titanite), but there is no petrographic or geochemical evidence that garnet was involved. Rutile is stable at pressure >1.5 GPa and melting with rutile residue can generate negative Nb-Ta anomalies (e.g., Xiong et al., 2005). The ratio of D_{Nb}/D_{Ta} in the rutile/melt system is 0.67 to 0.78, showing that rutile prefers Ta relative to Nb (Gao et al., 2007; Xiong et al., 2005). Therefore, melts generated from a source with rutile residue will have negative Nb and Ta anomalies and high ratios of Nb/Ta. Xiong et al. (2005) showed that oceanic adakites without rutile residue in the source have low Nb/Ta ratios compared to continental adakites. Amphibole is the second important silicate mineral capable of fractionating Nb, Ta and Ti (Li et al., 2017). For amphibole D_{Nb} = 0.16–0.90, D_{Ta} = 0.13–0.68, D_{Ti} = 1.81–10.63 and D_{Nb}/D_{Ta} = 0.76–2.82 (Li et al., 2017). Therefore, amphibole residue or extreme fractional

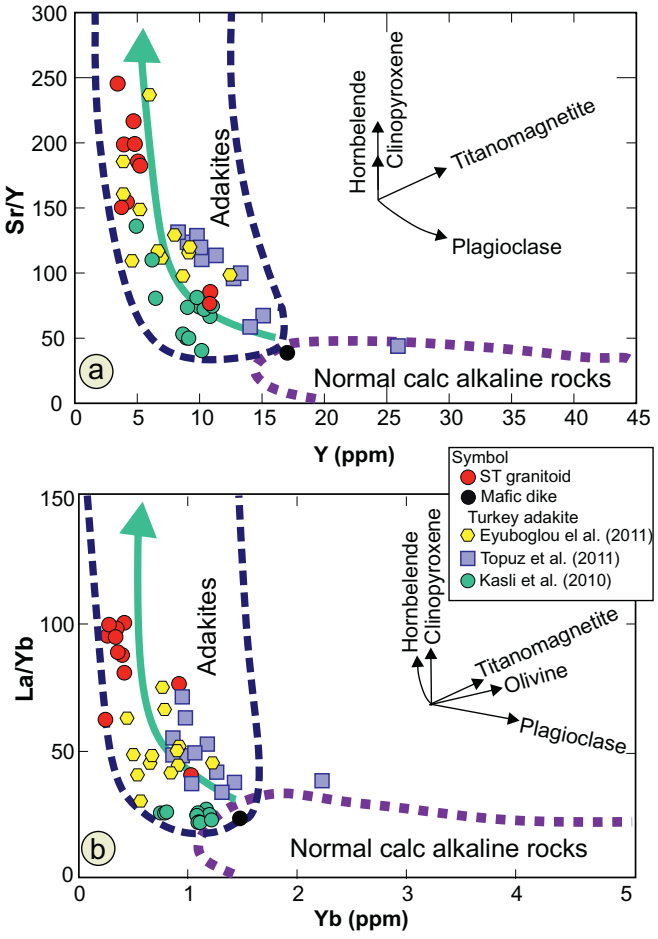

Fig. 9. (a) Sr/Y vs. Y and (b) La/Yb vs. Yb diagram for ST and Turkish Pontide granitic rocks. These granitoids plot in the adakite field in the Sr/Y versus the Y and La/Yb versus the Yb diagrams (Defant and Drummond, 1990). Distribution of the samples around the green arrow line confirms an important role for hornblende-controlled magmatic differentiation (Castillo, 2012). The samples TG-1 (490) and TG-4 show unusually high Sr/Y ratios, 490 and 895 respectively and we filtered out these two samples to plot in the figure (a) diagram and also sample TG-4 with high La/Yb ratio (350) was not plotted in the figure(b).

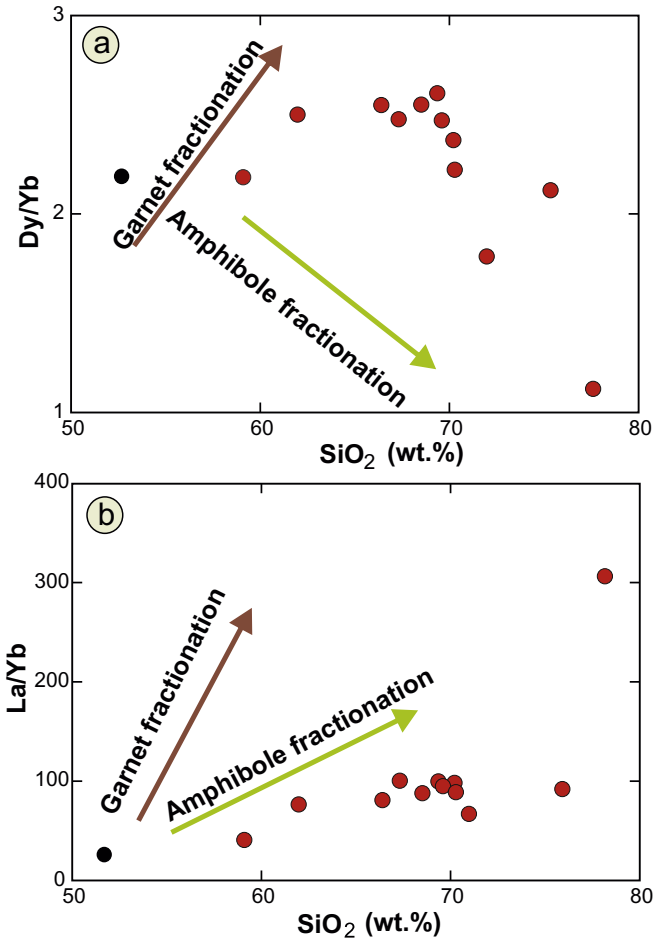

Fig. 10. Variation of Dy/Yb and La/Yb ratios versus SiO_2 (wt%) contents, showing decreasing Dy/Yb ratios and increasing La/Yb ratios (a, b) which are more consistent with ST granitoid fractionation controlled by amphibole rather than garnet. Garnet and amphibole trends from Davidson et al. (2007).

crystallization can also make negative Nb, Ta, and Ti anomalies in resultant magmas. Amphibole also has high partition coefficients for the HREEs (Li et al., 2017).

The low abundances of HREE and Ti in ST granitoids may be related to amphibole and rutile stability in the magma source region or magma reservoir. Zr is mainly concentrated in zircon, also some in amphibole and garnet in high-grade metamorphic rocks, with amphibole hosting more Zr compared to garnet (Fraser et al., 1997). The low contents of TiO_2, Sm, and Zr and high Na/Ta in the ST igneous rocks and the lack

Table 3
Isotope ratios of the ST granitoid and mafic dike.

Sample	$^{87}Sr/^{86}Sr$	1 SE	$^{143}Nd/^{144}Nd$	1 SE	$^{87}Rb/^{86}Sr$	$^{147}Sm/^{144}Nd$	$^{87}Sr/^{86}Sr(i)$	$^{143}Nd/^{144}Nd(i)$	εNd (t)	T_{DM} (Ga)
TG-1	0.705475	0.000007	0.512446	0.000075	0.257	0.065	0.7053	0.51242	−2.8	0.70
TG-2	0.704831	0.000006	0.512623	0.000006	0.172	0.082	0.7047	0.51259	0.5	0.59
TG-3	0.705028	0.000007	0.512609	0.000006	0.383	0.079	0.7047	0.51258	0.3	0.59
TG-4	0.705854	0.000006	0.512609	0.000006	1.49	0.050	0.7047	0.51259	0.5	0.49
TG-5 (Mafic dike)	0.705579	0.000008	0.512529	0.000004	0.250	0.099	0.7054	0.51249	−1.4	0.79
TG-6	0.705494	0.000006	0.512593	0.000004	0.268	0.091	0.7053	0.51256	−0.1	0.67
TG-7	0.704917	0.000005	0.512626	0.000004	0.252	0.073	0.7047	0.51260	0.7	0.55
TG-8	0.705191	0.000006	0.512627	0.000005	0.375	0.078	0.7049	0.51260	0.7	0.57
TG-9	0.704882	0.000006	0.512624	0.000004	0.265	0.078	0.7047	0.51260	0.6	0.57
TG-10	0.704971	0.000007	0.512628	0.000004	0.304	0.077	0.7047	0.51260	0.7	0.56
TG-11	0.704901	0.000007	0.512631	0.000017	0.290	0.076	0.7047	0.51260	0.7	0.55
TG-12	0.704934	0.000006			0.276	0.070	0.7047			
TG-13	0.704709	0.000006	0.512699	0.000004	0.384	0.079	0.7044	0.51267	2.0	0.49

The Nd and Sr natural isotope ratios were normalized based on the $^{146}Nd/^{144}Nd = 0.7219$ and $^{86}Sr/^{88}Sr = 0.1194$. Averages and 1 SE for isotope ratio standards, JNdi-1 and NIST-SRM987, are $^{143}Nd/^{144}Nd = 0.512112 \pm 0.000001$ ($n = 2$) and $^{87}Sr/^{86}Sr = 0.710263 \pm 0.000010$ ($n = 4$). The CHUR (Chondritic Uniform Reservoir) values, $^{147}Sm/^{144}Nd = 0.1967$ and $^{143}Nd/^{144}Nd = 0.512638$, were used to calculate the εNd(t) (DePaolo and Wasserburg, 1979). The BABI (Basaltic Achodritic Best Initial) value, $^{87}Sr/^{86}Sr = 0.69899$, and $^{87}Rb/^{86}Sr$ ratios of UR (undifferentiated reservoir) = 0.0827 were used.
$T_{DM} = 1/\lambda * \ln[(^{143}Nd/^{144}Nd_{sample}\text{-}0.512{,}638)/(^{147}Sm/^{144}Nd_{sample}\text{-}0.2137) + 1]$ (Jahn et al., 1999): $\lambda = 6.54 * 10^{-12}\ y^{-1}$.
p: present; i: initial ratio.

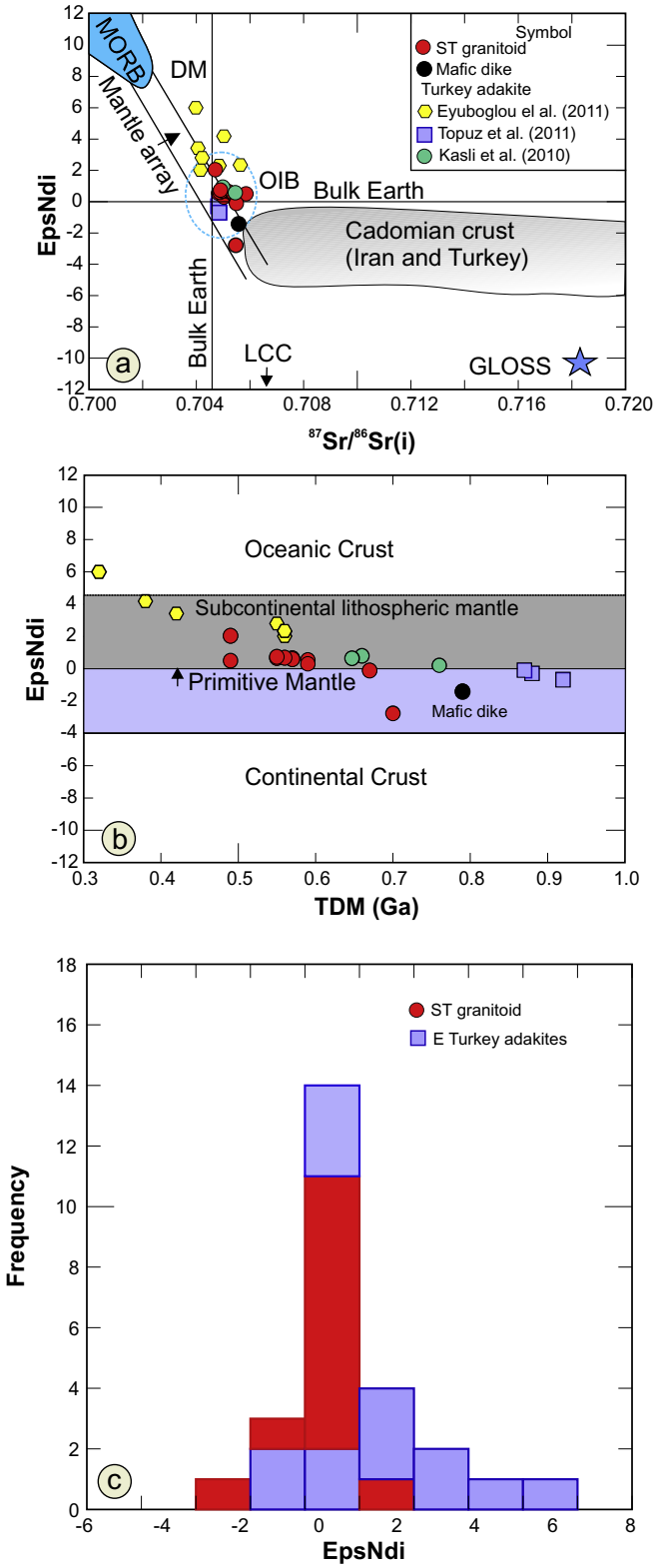

Fig. 11. (a) $^{87}Sr/^{86}Sr_{(i)}$ versus $\varepsilon_{Nd}(t)$ for NW Iran and eastern Turkey Paleogene adakitic rocks showing that both suites plot in the mantle array. (b) Some samples with positive $\varepsilon_{Nd}(t)$ plot in the depleted mantle and are isotopically distinguished from Iranian continental crust. (c) Peak of histogram of $\varepsilon_{Nd}(t)$ is situated around 0 to +1 and is skewed to higher values (depleted mantle). Skewness with asymmetric shape confirms that both minor continental crust component and melts from depleted mantle combined to generate the adakite magmas in this zone. Data for Cadomian crustal basement of Iran is from Badr et al. (2018), Shabanian et al. (2018) and Shafaii Moghadam et al. (2017) and Turkey (Stern et al., 2016; Ustaömer et al., 2009). *Abbreviations: DM = Depleted mantle, OIB = Oceanic Island basalt, LCC = Lower continental crust, GLOSS = Global subducted sediments* (Plank and Langmuir, 1998).

of negative Lu and Yb anomalies support the main role of amphibole for evolution of ST granitoid melts. Plots of Dy/Yb and La/Yb versus SiO_2 (wt%) contents (Davidson et al., 2007) clearly shows decreasing Dy/Yb and increasing La/Yb with SiO_2, relationships which are consistent with amphibole control for these magmas (Fig. 10a, b).

There is little variability in the Sr and Nd isotopic compositions of the ST rocks, including mafic dike and granitoids, indicating that assimilation of continental crust was of minor importance. $^{87}Sr/^{86}Sr$ (i) versus $\varepsilon_{Nd}(t)$ plot for the ST igneous rocks, along with the compiled data for similar rocks from NE Turkey show that some samples have slightly positive $\varepsilon_{Nd}(t)$ values suggesting derivation from slightly depleted mantle (Fig. 11a). These adakites are mostly isotopically different from exposed Iranian continental crust, especially for $^{87}Sr/^{86}Sr(i)$ (Fig. 11b), although some samples have isotopic compositions that overlap with the Cadomian basement of Iran. These samples have isotopic compositions expected for Cadomian subcontinental lithospheric mantle. The $\varepsilon_{Nd}(t)$ histogram is centered on 0 to 1 and skewed to higher values of $\varepsilon_{Nd}(t)$ (depleted mantle; Fig. 11c). Coupled variations of $^{87}Sr/^{86}Sr(i)$ and $\varepsilon_{Nd}(t)$ suggest that adakitic magmas were mostly derived from partial melting of subcontinental lithospheric mantle with minor assimilation of lower continental crust.

3.2. Petrogenesis of high-K adakite

The ST granitoids are metaluminous to peraluminous (Fig. 12a) and plot in the fields of volcanic arc to *syn*-collision granitoids (Pearce et al., 1984, Fig. 12 b, c). Furthermore, the samples plot in the active continental margin field based on the Th/Yb and Nb/Yb ratios (Schandl and Gorton, 2002, Fig. 12d–f). All these suggest that the ST granitoid formed at an active continental margin. The ST granitoids contain low abundances of MgO, CaO, Na_2O, Cr, and Ni, but high abundances of SiO_2, and are therefore, classified as high silica adakites (Fig. 13a, b) (Martin et al., 2005). The ST granitoids have geochemical and isotopic signatures which differ from those of adakites generated by partial melting of thickened continental crust or subducted oceanic crust. For example, continental crust-derived adakitic rocks have low $\varepsilon_{Nd}(t)$ values, whereas oceanic-slab derived adakites have high $\varepsilon_{Nd}(t)$ values. ST granitoids have high K_2O/Na_2O ratio (0.5–1.1) but variable $\varepsilon_{Nd}(t)$ values. Nearly, horizontal HREEs patterns for ST granitoids indicate that garnet did not play a major role in in the source and through the course of igneous crystallization. Low contents of MgO, Ni, Cr, and V in the ST granitoids are inconsistent with direct mantle melting or reaction of oceanic and/or orogenic type adakite melts with mantle. Instead, hornblende fractionation and minor assimilation of crust probably generated the ST granitoids. Mafic input from partial melting of hydrous subcontinental lithosphere above a subduction zone was the ultimate cause of this magmatic system. Other possibilities such as partial melting of alkali basalt (Sen and Dunn, 1994) or differentiation of high-K basaltic magma at high pressure conditions have been suggested for similar rocks (Ghiorso et al., 2002).

At pressure >2 GPa and temperature ~1070 °C, clinopyroxene becomes increasingly omphacitic. In this environment, Na is incorporated into residual clinopyroxene and K-rich melts can be produced (Xiao and Clemens, 2007). This process is more likely with collision-related thickening of continental crust to >70 km thick, as is suggested for collision-related adakites (Chung et al., 2003). Detachment of high-pressure eclogites from the lower crust during orogenic collapse and sinking of these rocks into the mantle as eclogitic drips that are melted may explain the genesis of some high-K adakites (Xiao and Clemens, 2007).

Experimental studies (Ma et al., 2015; Qian and Hermann, 2013) indicate that source rock composition has an essential role for generating different types of adakite magmas and that this can occur in crust <50 km thick. Qian and Hermann (2013) showed

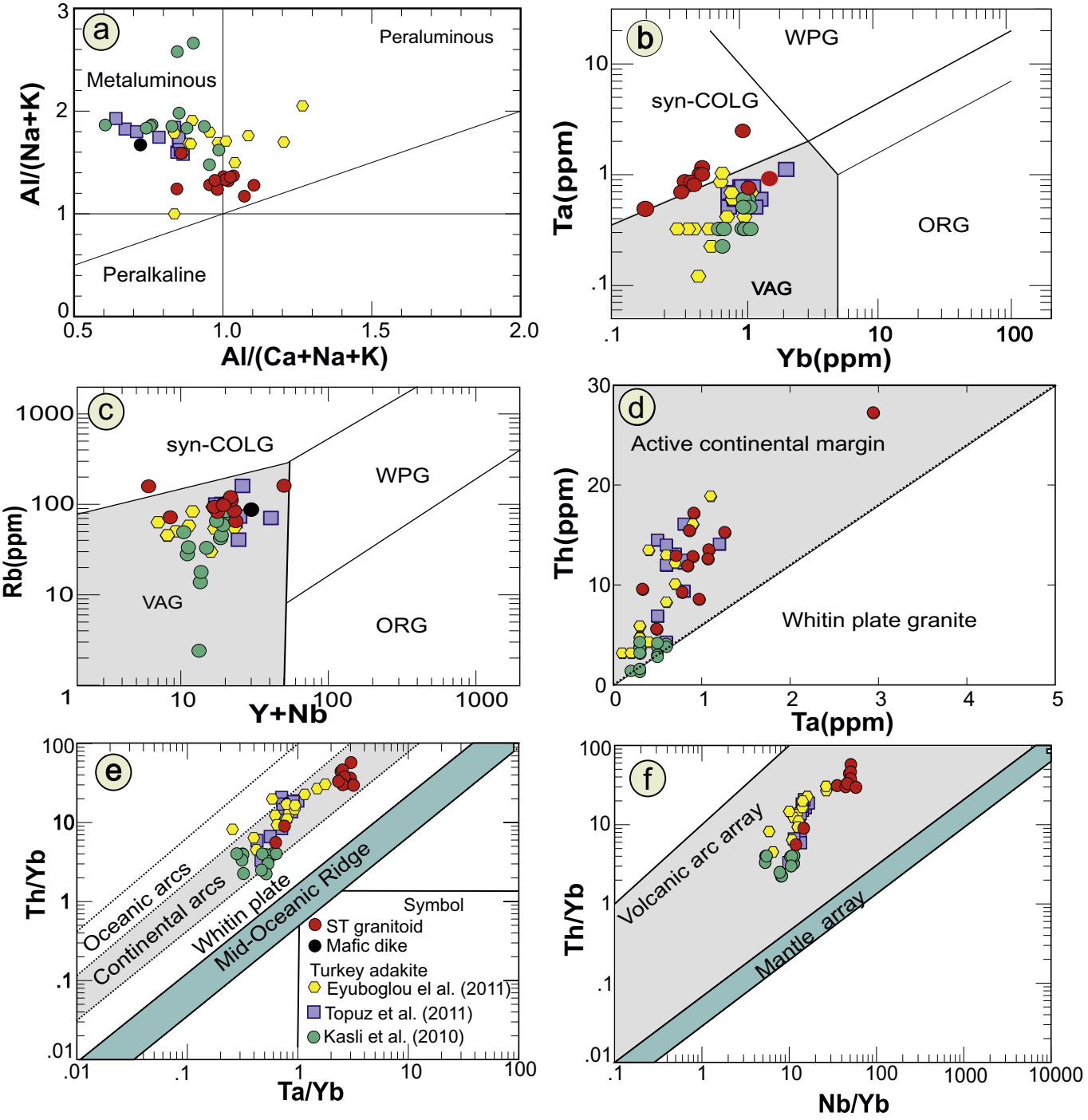

Fig. 12. Tectonic discrimination diagrams. All samples plot in the metaluminous to peraluminous field in the Shand diagram (a), in volcanic arc to *syn*-collision fields in the granite tectonic setting diagrams (c, d: Pearce et al., 1984) and in active continental margin in the tectonic discrimination diagram for granites (d-f: Schandl and Gorton, 2002).

that 10–40% partial melting of hydrous metabasaltic lower crust at 10–12.5 kbar (33–41 km depth) and 800–950 °C can produce adakitic melts, leaving a residue of garnet amphibolite, two-pyroxene granulite or garnet-bearing granulite. Dai et al. (2017) based on the rhyolite -MELT system argued that magmatic Sr/Y and La/Yb ratios mainly are controlled by plagioclase and garnet in residue respectively. High pressure melts have higher ratios of Sr/Y and La/Yb whereas lower pressure melts have lower ratios. Based on their model, orogenic adakites with ratios of Sr/Y > 300 and continental adakites with Sr/Y < 200 can be generated at different depths in the continental crust. These processes are regarded as unlikely for the genesis of the ST granitoids.

The crystallization of mafic magmas in the lower continental crust is another mechanism for generating continental adakites. In this case, the amphibole + garnet-dominated fractional crystallization of mantle-derived magmas within normal crust (i.e., 41 km; Christensen and Mooney, 1995) can make adakitic melts with Sr/Y ratios around 200 or lower. On the Yb_{SN} versus $(Sm/Yb)_{SN}$ and Nb/La versus Ba/Th ratio diagrams (SN = source normalized data mafic lower continental crust with Yb = 1.5 ppm and Sm/Yb = 1.87 for continental adakite, Ma et al., 2015) the ST and NE Turkey adakites plot in the low pressure adakite group (Fig. 14a, b). Low pressure adakite – generated by partial melting of lower continental crust or differentiated from amphibole-dominated fractionation of

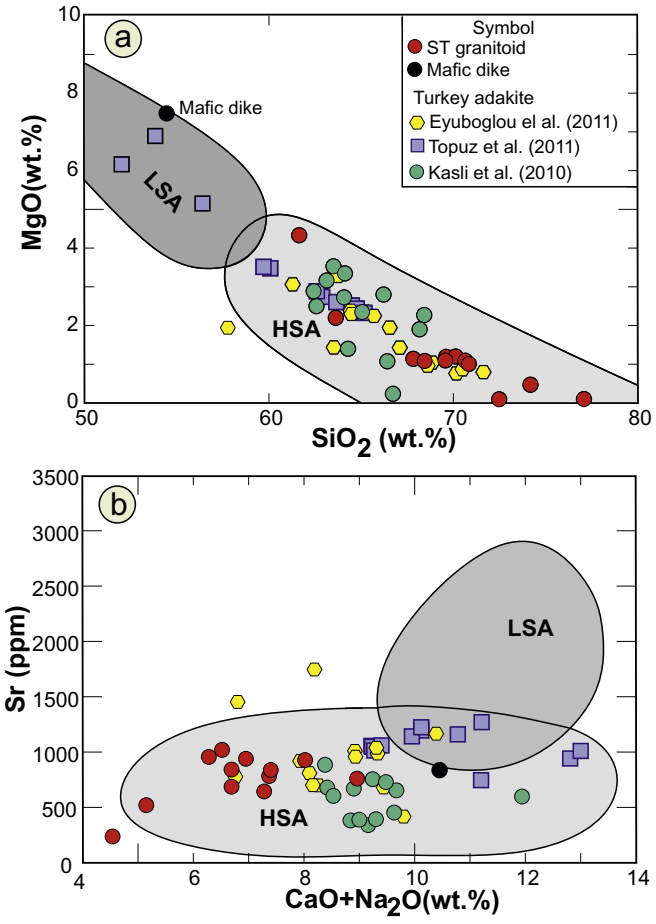

Fig. 13. Classification schemes for low-silica adakites (LSA) and high-silica adakites (HSA) (Martin et al., 2005). All Paleocene adakites in northwest Iran and most from eastern Turkey plot in the high silica adakite fields.

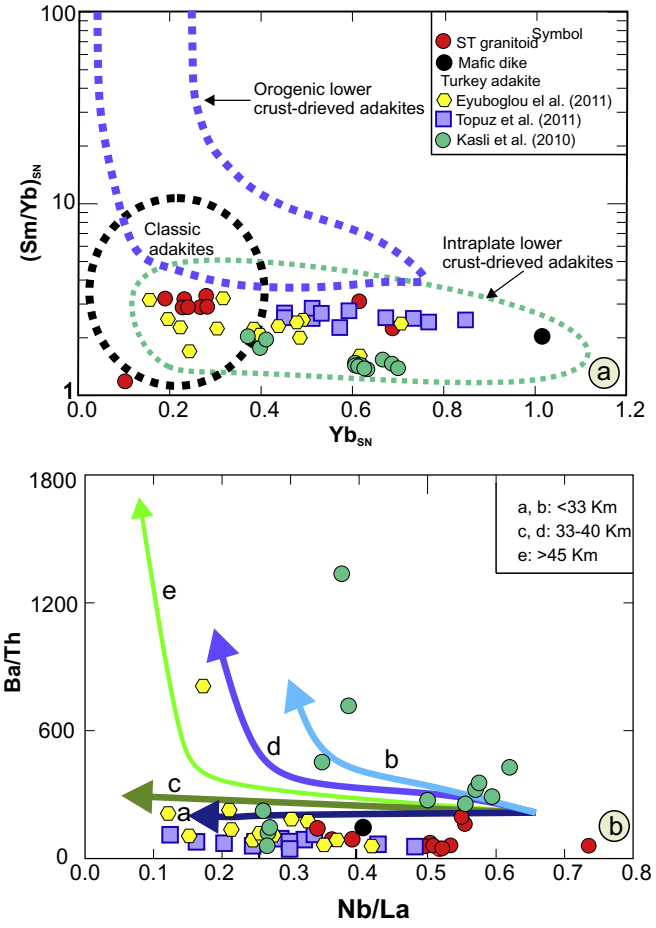

Fig. 14. Normalized compositions of ST granitoid and eastern Pontides adakites with typical composition of the lower crust (SN = source normalized data; normalized to mafic lower continental crust with Yb = 1.5 ppm and Sm/Yb = 1.87 for continental adakite (Ma et al., 2015)). Paleocene adakitic rocks plotted on the (a) Yb_{SN} versus $(Sm/Yb)_{SN}$ and (b) Ba/Th vs. Nb/La diagram (Dai et al., 2017; Ma et al., 2015) showing that most samples cluster around the lower pressure line (a; <33 km) confirming the generation of Paleogene adakites by processes associated with continental crust of near-normal thickness.

calc-alkaline magma - shows lower Ba/Th and $(Sm/Yb)_{SN}$ compared to oceanic and orogenic adakites (Fig. 14a, b).

3.3. Geodynamics and crustal evolution

Our new U-Pb zircon ages show that the ST granitoids are the first known examples of Paleogene adakitic rocks in northwest Iran. Similar Paleocene-Early Eocene adakitic rocks (medium-K quartz diorites to leuco-granites) are common in the Pontides (eastern Turkey), north of the Izmir-Ankara-Erzincan suture (e.g., Topuz et al., 2005, 2011; Karsli et al., 2010; Eyüboglu et al., 2011). It is useful to compare these related igneous rocks to see if these can be understood as a single magma-genetic system.

Topuz et al. (2011) reported Early Eocene (52 Ma) adakites near Ağvanis in NE Turkey with initial $\varepsilon_{Nd}(t)$ values of +1.0 to −1.1 and $^{87}Sr/^{86}Sr$ ratios of 0.7042 to 0.7049 and suggested that these resulted from partial melting of thickened continental crust following orogenic collapse of the Pontides during Paleocene time. Paleocene adakites (~56 Ma) are also common in the eastern Pontides, around Kop Mountain (Erzurum– Erzincan). These adakites have higher $\varepsilon_{Nd}(t)$ values (+2.3 to +4.9) and initial ratios of $^{87}Sr/^{86}Sr$ (0.7041 to 0.7055). Hornblende differentiation has been suggested for the genesis of these adakites (Eyüboglu et al., 2011). The $\varepsilon_{Nd}(t)$ values and $^{87}Sr/^{86}Sr_{(i)}$ ratios of Paleocene -Early Eocene adakites from both Turkey and northwest Iran mostly follow the mantle array (Fig. 12a). Young T_{DM} ages (400–600 Ma) for the ST granitoids are broadly consistent with participation of Cadomian lower crust and/or subcontinental lithospheric mantle (SCLM) to form these magmas; only minor crust involvement is allowed by low $^{87}Sr/^{86}Sr$ ratios and by the isotopic similarity of mafic and felsic igneous rocks. The isotopic compositions of these adakites differ significantly from those of Iranian Cadomian continental crust (Badr et al., 2018; Shabanian et al., 2018; Shafaii Moghadam et al., 2017; Fig. 11a), but allow for some contributions from this as well as subducted sediments. Moderate and variable $\varepsilon_{Nd}(t)$ values for these adakitic rocks (−1 to +5) attest that these rocks are dominated by contributions from subcontinental lithospheric mantle (SCLM) but there may also be significant contributions from asthenospheric mantle. The low $^{87}Sr/^{86}Sr_{(i)}$ ratios and minor positive $\varepsilon_{Nd}(t)$ also overlap with non-adakitic, calc-alkaline igneous rocks in the region. There is no evidence for unusually thick crust in this area.

We suggest two scenarios for the generation of Late Paleocene adakitic magmas in NW Iran. The first is that N-SaSZ crust was thickened as a result of the collision of the Arabian plate and the N-SaSZ block in the Late Cretaceous, followed by collapse and delamination of lower crust rocks (metamorphosed in high-P conditions) into the hot mantle, similar to what is suggested for adakites from eastern Turkey (e.g., Topuz et al., 2005, 2011; Karsli et al., 2010; Eyüboglu et al., 2011). This hypothesis has some problems; for example, if the collision occurred at ~70 Ma ago, the time interval for the thickening of this crust (~ 100 km distant from the Zagros suture zone), and thereafter delamination and partial melting to produce adakite melts is quite short. Also, there is little evidence for such an early time of collision and no support

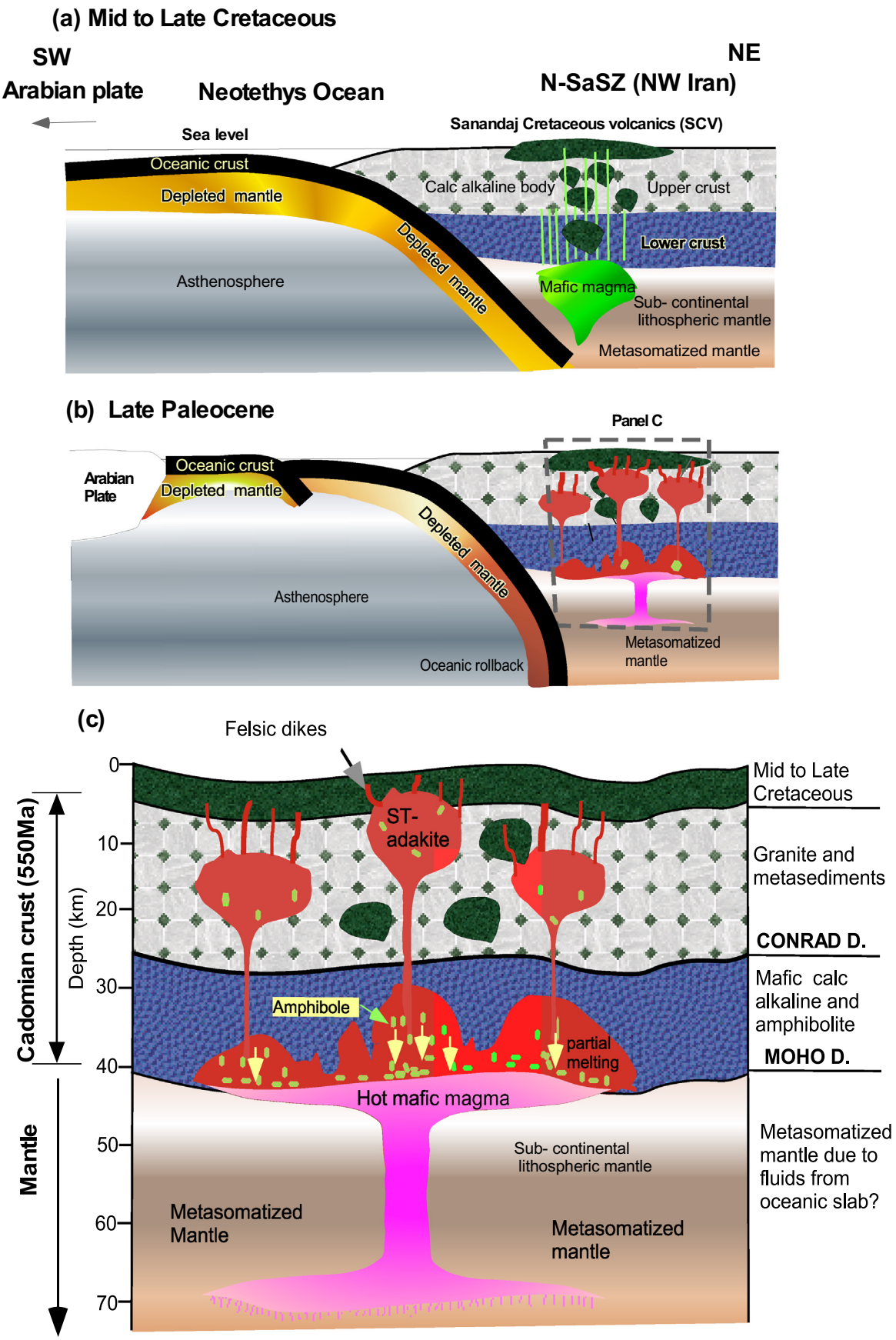

Fig. 15. (a-c) Simplified sketches for the evolution of ST granitoid in NW Iran and E Turkey. (a) Development of Cretaceous alkaline volcanic rocks in the northern Sanandaj (SCV) in an active continental margin (Azizi and Jahangiri, 2008) due to Neotethys subduction beneath the SaSZ. (b-c) Trigger for intra-oceanic arc systems and roll back activities of the Neotethys oceanic crust beneath the SaSZ following upwelling of hot asthenosphere melts and emplacement of mafic magma in the basal of continental crust in the NW Iran. The injection of hot basaltic magma leading to partial melting of lower crust mafic calc alkaline bodies. Fractionation of amphiboles increases magmatic silica, alkali elements and LREE contents further, resulting in differentiated magma with high-K adakite composition.

from geophysical data for greatly thickened crust beneath NW Iran. Gravimetric and seismic studies show that the continental crust in this area is 42–46 km thick (Mooney et al., 1998; Taghizadeh-Farahmand et al., 2015). Furthermore, the Paleogene was a time of crustal thinning in Iran, not thickening, as shown by the presence of many core complexes and rift basins of Eocene-Oligocene age, including a submarine rift along the Iran-Iraq border (Ali et al., 2013; Azizi et al., 2011;Azizi and Moinevaziri, 2009; Nouri et al., 2016). Furthermore, the 37–40 Ma Baneh granite-appinite syntectonic complex implies that collision did not begin in this part of Iran until late Eocene time (Azizi et al., 2019).

The second scenario emphasizes heating of N-SaSZ lithospheric mantle and partial melting to generate non-adakitic calc-alkaline basaltic magma and thereafter extensive amphibole (±titanite ±rutile) fractionation produced the final adakitic magmas. Eocene magmatic rocks are widely reported in the Zagros suture zone along the Iraq-Iran border as expressions of convergent margin igneous activity (Azizi and Moinevaziri, 2009; Nouri et al., 2016). The chemical composition and isotope ratios of these rocks clearly confirm operation of a vigorous arc - backarc magmatic system in Eocene time in the western part of the N-SaSZ, which is known as the Songhor Baneh volcano- plutonic belt (SBV, Azizi and Moinevaziri, 2009; Ali et al., 2013). The development of three parallel volcanic belts (Sanandaj Cretaceous volcanic (SCV), Songor Baneh volcano-plutonic (SBV) and Hamadan Tabriz volcanic (HTV), Fig. 1), Cretaceous in the center (SCV belt; Azizi and Jahangiri, 2008), Eocene in the west (SBV) and Miocene-Pliocene (HTV belt) in the eastern part of the N-SaSZ (Fig. 1), confirms that the northern SaSZ has been the locus of arc igneous activity over the past 100 Ma. During Oligocene time and later, numerous extensional basins formed and filled with conglomerates, sandstones and limestones (Fig. 2) but no such basins are reported for Paleocene-Eocene sedimentation in that area, suggesting that this crust was thicker. The crust beneath the Saqqez-Takab region is ~46–41 km thick, slightly thicker than normal continental crust (41 km). This may reflect the slightly greater thickness of the crust due to Cretaceous magmatic activities indicating that Paleogene extension did not affect this region as much as it affected other parts of Iran.

We suggest that rollback of the Neotethys oceanic slab in the Late Cretaceous-Paleocene led to upwelling of hot asthenosphere beneath NW Iran, leading to hydrous partial melting of subcontinental lithospheric mantle to generate mafic calc-alkaline magmas. Fractionation of hornblende from these magmas or melting of old calc-alkaline rocks emplaced in the lower crust produced K-rich adakitic granitoid in northwest Iran and E Turkey. Our schematic model is summarized in Fig. 15(a–c).

4. Conclusions

The Saqqez-Takab granitoids of NW Iran display high-K adakitic signature, characterized by high Sr/Y, La/Yb and K_2O/Na_2O ratios. U-Pb zircon ages indicate formation during the Paleocene. This is the first documented occurrence of Paleogene adakites in Iran. These granitoids are similar to Late Paleocene-Early Eocene adakites in NE Turkey. Our geochemical and isotopic data confirm that these adakitic rocks were not generated from partial melting of subducted oceanic crust or by lower crust partial melting of greatly thickened continental crust in a collision zone. We suggest that the ST granitoids and NE Turkey adakites were produced in association with slightly thickened continental crust as a result of combined amphibole-dominated fractionation of calc-alkaline magma directly and or melting of old calc-alkaline bodies which has emplaced in the lower crust. The restricted location where these melts were generated in Late Paleocene-Early Eocene time and the absence of other adakitic rocks in NW Iran until the late Miocene reinforces these conclusions.

Supplementary data to this article can be found online at https://doi.org/10.1016/j.lithos.2019.105151.

Acknowledgements

Fieldwork and sampling were supported by the Geological Survey of Iran, Sanandaj-Branch. We thank F. Rezaei, S. Gholipour and Z. Abbasi for assistance with fieldwork. H. Azizi thanks Kurdistan University and Nagoya University for supporting his sabbatical studies in 2017-2018. Analytical studies were supported by Japan Society for Promotion of the Science (JSPS) KAKENHI grant number 17H01671. This version is much improved based on critical comments by two anonymous reviewers and Şenel Özdamar and also editors Neslon Eby and Michael Roden. This is UTD Geosciences contribution number 1331.

References

Abdulzahra, I.K., Hadi, A., Asahara, Y., Azizi, H., Yamamoto, K., 2016. Zircon U–Pb ages and geochemistry of Devonian A-type granites in the Iraqi Zagros Suture Zone (Damamna area): new evidence for magmatic activity related to the Hercynian orogeny. Lithos 264, 360–374.

Abdulzahra, I.K., Hadi, A., Asahara, Y., Azizi, H., Yamamoto, K., 2018. Petrogenesis and geochronology of Mishao peraluminous I-type granites, Shalair valley area, NE Iraq. Chemie der Erde Geochem. 78, 215–227.

Ali, S.A., Buckman, S., Aswad, K.J., Jones, B.G., Ismail, S.A., Nutman, A.P., 2013. The tectonic evolution of a Neo-Tethyan (Eocene-Oligocene) island-arc (Walash and Naopurdan groups) in the Kurdistan region of the Northeast Iraqi Zagros Suture Zone. Island Arc 22, 104–125.

Azizi, H., Jahangiri, A., 2008. Cretaceous subduction-related volcanism in the northern Sanandaj-Sirjan Zone, Iran. J. Geodyn. 45, 178–190.

Azizi, H., Moinevaziri, H., 2009. Review of the tectonic setting of cretaceous to Quaternary volcanism in northwestern Iran. J. Geodyn. 47, 167–179.

Azizi, H., Asahara, Y., Mehrabi, B., Chung, S.L., 2011. Geochronological and geochemical constraints on the petrogenesis of high-K granite from the Suffiabad area, Sanandaj-Sirjan Zone NW Iran. Chem. der Erde-Geochem. 71, 363–376.

Azizi, H., Asahara, Y., Tsuboi, M., Takemura, K., Razyani, S., 2014. The role of heterogenetic mantle in the genesis of adakites northeast of Sanandaj, northwestern Iran. Chem. Erde-Geochem. 74, 87–97.

Azizi, H., Zanjefili-Beiranvand, M., Asahara, Y., 2015. Zircon U–Pb ages and petrogenesis of a tonalite–trondhjemite–granodiorite (TTG) complex in the northern Sanandaj–Sirjan zone, Northwest Iran: evidence for late Jurassic arc–continent collision. Lithos 216, 178–195.

Azizi, H., Kazemi, T., Asahara, Y., 2017. A-type granitoid in Hasansalaran complex, northwestern Iran: evidence for extensional tectonic regime in northern Gondwana in the late Paleozoic. J. Geodyn. 108, 56–72.

Azizi, H., Hadad, S., Stern, R.J., Asahara, Y., 2019. Age, geochemistry, and emplacement of the~ 40-Ma Baneh granite–appinite complex in a transpressional tectonic regime, Zagros suture zone, Northwest Iran. Int. Geol. Rev. 61, 195–223.

Badr, A., Davoudian, A.R., Shabanian, N., Azizi, H., Asahara, Y., Neubauer, F., Dong, Y., Yamamoto, K., 2018. A-and I-type metagranites from the North Shahrekord Metamorphic complex, Iran: evidence for early Paleozoic post-collisional magmatism. Lithos 300, 86–104.

Bea, F., Mazhari, A., Montero, P., Amini, S., Ghalamghash, J., 2011. Zircon dating, Sr and Nd isotopes, and element geochemistry of the Khalifan pluton, NW Iran: evidence for Variscan magmatism in a supposedly Cimmerian super terrane. J. Asian Earth Sci. 40, 172–179.

Castillo, P.R., 2006. An overview of adakite petrogenesis. Chin. Sci. Bull. 51, 257–268.

Castillo, P.R., 2012. Adakite petrogenesis. Lithos 134–135, 304–316.

Castillo, P.R., Janney, P.E., Solidum, R.U., 1999. Petrology and geochemistry of Camiguin Island, southern Philippines: insights to the source of adakites and other lavas in a complex arc setting. Contrib. Mineral. Petrol. 134, 33–51.

Christensen, N.I., Mooney, W.D., 1995. Seismic velocity structure and composition of the continental crust: a global view. J. Geophys. Res. Solid Earth 100 (B6), 9761–9788.

Chung, S.L., Liu, D., Ji, J., Chu, M.F., Lee, H.Y., Wen, D.J., Lo, C.H., Lee, T.Y., Qian, Q., Zhang, Q., 2003. Adakites from continental collision zones: melting of thickened lower crust beneath southern Tibet. Geology 31, 1021–1024.

Coldwell, B., Adam, J., Rushmer, T., Macpherson, C.G., 2011. Evolution of the East Philippine Arc: experimental constraints on magmatic phase relations and adakitic melt formation. Contrib. Mineral. Petrol. 162, 835.

Condie, K.C., 2005. TTGs and adakites: are they both slab melts? Lithos 80, 33–44.

Dai, H.-K., Zheng, J., Zhou, X., Griffin, W.L., 2017. Generation of continental adakitic rocks: crystallization modeling with variable bulk partition coefficients. Lithos 272–273, 222–231.

Davidson, J., Turner, S., Handley, H., Macpherson, C., Dosseto, A., 2007. Amphibole "sponge" in arc crust? Geology 35, 787–790.

Deevsalar, R., Shinjo, R., Ghaderi, M., Murata, M., Hoskin, P.W.O., Oshiro, S., Wang, K.L., Lee, H.Y., Neill, I., 2017. Mesozoic–Cenozoic mafic magmatism in Sanandaj–Sirjan Zone, Zagros Orogen (Western Iran): geochemical and isotopic inferences from middle jurassic and late eocene gabbros. Lithos 284, 588–607.

Defant, M.J., Drummond, M.S., 1990. Derivation of some modern arc magmas by melting of young subducted lithosphere. Nature 347, 662.

Delavari, M., Amini, S., Schmitt, A.K., McKeegan, K.D., Harrison, T.M., 2014. U–Pb geochronology and geochemistry of Bibi-Maryam pluton, eastern Iran: implication for the late stage of the tectonic evolution of the Sistan Ocean. Lithos 200, 197–211.

DePaolo, D.J., Wasserburg, G.J., 1979. Petrogenetic mixing models and Nd-Sr isotopic patterns. Geochim. Cosmochim. Acta 43, 615–627.
Eyüboglu, Y., Santosh, M., Chung, S.L., 2011. Crystal fractionation of adakitic magmas in the crust–mantle transition zone: petrology, geochemistry and U–Pb zircon chronology of the Seme adakites, Eastern Pontides, NE Turkey. Lithos 121, 151–166.
Fraser, G., Ellis, D., Eggins, S., 1997. Zirconium abundance in granulite-facies minerals, with implications for zircon geochronology in high-grade rocks. Geology 25, 607–610.
Gao, S., Rudnick, R.L., Yuan, H.L., Liu, X.M., Liu, Y.S., Xu, W.L., Ling, W.L., Ayers, J., Wang, X.C., Wang, Q.H., 2004. Recycling lower continental crust in the North China craton. Nature 432, 892.
Gao, J., John, T., Klemd, R., Xiong, X., 2007. Mobilization of Ti–Nb–Ta during subduction: evidence from rutile-bearing dehydration segregations and veins hosted in eclogite, Tianshan, NW China. Geochim. Cosmochim. Acta 71, 4974–4996.
Ghiorso, M.S., Hirschmann, M.M., Reiners, P.W., Kress III, V.C., 2002. The pMELTS: a revision of MELTS for improved calculation of phase relations and major element partitioning related to partial melting of the mantle to 3 GPa. Geochem. Geophys. Geosyst. 3, 1–35.
Ghorbani, M.R., Bezenjani, R.N., 2011. Slab partial melts from the metasomatizing agent to adakite, Tafresh Eocene volcanic rocks, Iran. Island Arc 20, 188–202.
Hariri, A., Farjandi, F., Vaezipoor, M., Sadegi, A., 2003. Geology map of Saqqez. Geol. Surv. Iran. 5262.
Hassanzadeh, J., Stockli, D.F., Horton, B.K., Axen, G.J., Stockli, L.D., Grove, M., Schmitt, A.K., Walker, J.D., 2008. U-Pb zircon geochronology of late Neoproterozoic–early Cambrian granitoids in Iran: implications for paleogeography, magmatism, and exhumation history of Iranian basement. Tectonophysics 451, 71–96.
Hastie, A.R., Kerr, A.C., McDonald, I., Mitchell, S.F., Pearce, J.A., Millar, I.L., Barfod, D., Mark, D.F., 2010. Geochronology, geochemistry and petrogenesis of rhyodacite lavas in eastern Jamaica: a new adakite subgroup analogous to early Archaean continental crust? Chem. Geol. 276, 344–359.
Jahangiri, A., 2007. Post-collisional Miocene adakitic volcanism in NW Iran: geochemical and geodynamic implications. J. Asian Earth Sci. 30, 433–447.
Jahn, B.M., Wu, F., Lo, C.H., Tsai, C.H., 1999. Crustal-mantle interaction induced by deep subduction of the continental crust: geochemical and Sr–Nd isotopic evi- dence from post-collision mafic–ultramafic intrusions of the northern Dabie complex, Central China. Chem. Geol. 157, 119–1141.
Karsli, O., Dokuz, A., Uysal, İ., Aydin, F., Kandemir, R., Wijbrans, J., 2010. Generation of the early Cenozoic adakitic volcanism by partial melting of mafic lower crust, Eastern Turkey: implications for crustal thickening to delamination. Lithos 114, 109–120.
Li, Y.-B., Kimura, J.-I., Machida, S., Ishii, T., Ishiwatari, A., Maruyama, S., Qiu, H.N., Ishikawa, T., Kato, Y., Haraguchi, S., Takahata, N., Hirahara, Y., Miyazaki, T., 2013. High-Mg Adakite and Low-Ca Boninite from a Bonin Fore-arc Seamount: implications for the Reaction between Slab Melts and Depleted Mantle. J. Petrol. 54, 1149–1175.
Li, L., Xiong, X.L., Liu, X.C., 2017. Nb/Ta fractionation by amphibole in hydrous basaltic systems: implications for arc magma evolution and continental crust formation. J. Petrol. 58, 3–28.
Liu, S.A., Li, S., He, Y., Huang, F., 2010. Geochemical contrasts between early cretaceous ore-bearing and ore-barren high-Mg adakites in Central-Eastern China: implications for petrogenesis and Cu–au mineralization. Geochim. Cosmochim. Acta 74, 7160–7178.
Ma, Q., Zheng, J.P., Xu, Y.G., Griffin, W.L., Zhang, R.S., 2015. Are continental "adakites" derived from thickened or foundered lower crust? Earth Planet. Sci. Lett. 419, 125–133.
Mahmoudi, S., Corfu, F., Masoudi, F., Mehrabi, B., Mohajjel, M., 2011. U–Pb dating and emplacement history of granitoid plutons in the northern Sanandaj–Sirjan Zone, Iran. J. Asian Earth Sci. 41, 238–249.
Martin, H., 1999. Adakitic magmas: modern analogues of Archaean granitoids. Lithos 46, 411–429.
Martin, H., Smithies, R.H., Rapp, R., Moyen, J.F., Champion, D., 2005. An overview of adakite, tonalite–trondhjemite–granodiorite (TTG), and sanukitoid: relationships and some implications for crustal evolution. Lithos 79, 1–24.
Mazhari, S.A., Bea, F., Amini, S., Ghalamghash, J., Molina, J.F., Montero, P., Scarrow, J.H., Williams, I.S., 2009. The Eocene bimodal Piranshahr massif of the Sanandaj–Sirjan Zone, NW Iran: a marker of the end of the collision in the Zagros orogen. J. Geol. Soc. Lond. 166, 53–69.
Mazhari, S.A., Amini, S., Ghalamghash, J., Bea, F., 2011. Petrogenesis of granitic unit of Naqadeh complex, Sanandaj–Sirjan zone, NW Iran. Arab. J. Geosci. 4, 59–67.
Middlemost, E.A.K., 1994. Naming materials in the magma/igneous rock system. Earth-Sci. Rev. 37, 215–224.
Mooney, W.D., Laske, G., Masters, T.G., 1998. CRUST 5.1: a global crustal model at 5° × 5°. J. Geophys. Res. Solid Earth 103, 727–747.
Moyen, J.F., 2009. High Sr/Y and La/Yb ratios: the meaning of the "adakitic signature". Lithos 112, 556–574.
Nouri, F., Azizi, H., Golonka, J., Asahara, Y., Orihashi, Y., Yamamoto, K., Tsuboi, M., Anma, R., 2016. Age and petrogenesis of Na-rich felsic rocks in western Iran: evidence for closure of the southern branch of the Neo-Tethys in the late cretaceous. Tectonophysics 671, 151–172.
O'connor, J.T., 1965. A Classification for Quartz-Rich Igneous Rocks Based on Feldspar Ratios. US Geological Survey Professional Paper B 525, pp. 79–84.
Omrani, H., 2018. Island-arc and active continental margin adakites from the Sabzevar zone, Iran. Petrology 26, 96–113.
Pearce, J.A., Harison, N.B.W., Tindle, A.G., 1984. Trace element discrimination diagrams for the tectonic interpretation of granitic rocks. J. Petrol. 25, 956–983.
Peccerillo, A., Taylor, S.R., 1976. Geochemistry of Eocene calc-alkaline volcanic rocks from the Kastamonu area, northern Turkey. Contrib. Mineral. Petrol. 58, 63–81.
Plank, T., Langmuir, C.H., 1998. The chemical composition of subducting sediment and its consequences for the crust and mantle. Chem. Geol. 145, 325–394.
Qian, Q., Hermann, J., 2013. Partial melting of lower crust at 10–15 kbar: constraints on adakite and TTG formation. Contrib. Mineral. Petrol. 165, 1195–1224.
Rossetti, F., Nasrabady, M., Theye, T., Gerdes, A., Monié, P., Lucci, F., Vignaroli, G., 2014. Adakite differentiation and emplacement in a subduction channel: the late Paleocene Sabzevar magmatism (NE Iran). GSA Bull. 126, 317–343.
Schandl, E.S., Gorton, M.P., 2002. Application of high field strength elements to discriminate tectonic settings in VMS environments. Econ. Geol. 97, 629–642.
Sen, C., Dunn, T., 1994. Dehydration melting of a basaltic composition amphibolite at 1.5 and 2.0 GPa: implications for the origin of adakites. Contrib. Mineral. Petrol. 117, 394–409.
Shabanian, N., Davoudian, A.R., Dong, Y., Liu, X., 2018. U-Pb zircon dating, geochemistry and Sr-Nd-Pb isotopic ratios from Azna-Dorud Cadomian metagranites, Sanandaj-Sirjan Zone of western Iran. Precambrian Res. 306, 41–60.
Shafaii Moghadam, H., Stern, R.J., 2014. Ophiolites of Iran: keys to understanding the tectonic evolution of SW Asia: (I) paleozoic ophiolites. J. Asian Earth Sci. 91, 19–38.
Shafaii Moghadam, H., Li, X.H., Ling, X.X., Stern, R.J., Santos, J.F., Meinhold, G., Ghorbani, G., Shahabi, S., 2015. Petrogenesis and tectonic implications of late Carboniferous A-type granites and gabbronorites in NW Iran: Geochronological and geochemical constraints. Lithos 212–215, 266–279.
Shafaii Moghadam, H., Li, X.-H., Santos, J.F., Stern, R.J., Griffin, W.L., Ghorbani, G., Sarebani, N., 2017. Neoproterozoic magmatic flare-up along the N. margin of Gondwana: the taknar complex, NE Iran. Earth Planet. Sci. Lett. 474, 83–96.
Shahbazi, H., Siebel, W., Pourmoafee, M., Ghorbani, M., Sepahi, A.A., Shang, C.K., Abedini, M.V., 2010. Geochemistry and U–Pb zircon geochronology of the Alvand plutonic complex in Sanandaj–Sirjan Zone (Iran): new evidence for Jurassic magmatism. J. Asian Earth Sci. 39, 668–683.
Simpson, C., 1985. Deformation of granitic rocks across the brittle-ductile transition. J. Struct. Geol. 7, 503–511.
Stacey, J.S., Kramer, J.D., 1975. Approximation of the terrestrial lead isotope evolution by a two-stage model. Earth Planet. Sci. Lett. 26, 207–221.
Stern, C.R., Kilian, R., 1996. Role of the subducted slab, mantle wedge and continental crust in the generation of adakites from the andean Austral Volcanic Zone. Contrib. Mineral. Petrol. 123, 263–281.
Stern, R.A., Hanson, G.N., Shirey, S.B., 1989. Petrogenesis of mantle-derived, LILE-enriched archean monzodiorites and trachyandesites (sanukitoids) in southwestern superior province. Can. J. Earth Sci. 26, 1688–1712.
Stern, R.J., Ali, K.A., Ren, M., Jarrar, G.H., Romer, R.L., Leybourne, M.I., Whitehouse, M.J., Ibrahim, K.M., 2016. Cadomian (~560 Ma) crust buried beneath the northern Arabian Peninsula: mineral, chemical, geochronological, and isotopic constraints from NE jordan xenoliths. Earth Planet. Sci. Lett. 436, 31–42.
Stöcklin, J., 1974. Possible Ancient Continental margins in Iran. In: Burk, C.A., Drake, C.L. (Eds.), The Geology of Continental Margins. Springer, Berlin, Heidelberg.
Streckeisen, A., 1974. Classification and nomenclature of plutonic rocks recommendations of the IUGS subcommission on the systematics of igneous rocks. Geol. Rundsch. 63, 773–786.
Sun, S.S., McDonough, W.F., 1989. Chemical and isotopic systematics of oceanic basalts: implications for mantle composition and processes. Geol. Soc. Lond. Spec. Publ. 42, 313–345.
Taghizadeh-Farahmand, F., Afsari, N., Sodoudi, F., 2015. Crustal thickness of iran inferred from converted waves. Pure Appl. Geophys. 172, 309–331. https://doi.org/10.1007/s00024-014-0901-0.
Topuz, G., Altherr, R., Schwarz, W.H., Siebel, W., Satır, M., Dokuz, A., 2005. Post-collisional plutonism with adakite-like signatures: the eocene saraycik granodiorite (Eastern Pontides, Turkey). Contrib. Mineral. Petrol. 150, 441–455.
Topuz, G., Okay, A.I., Altherr, R., Schwarz, W.H., Siebel, W., Zack, T., Satır, M., Şen, C., 2011. Post-collisional adakite-like magmatism in the ağvanis massif and implications for the evolution of the eocene magmatism in the Eastern Pontides (NE Turkey). Lithos 125, 131–150.
Ustaömer, P.A., Ustaömer, T., Collins, A.S., Robertson, A.H., 2009. Cadomian (Ediacaran–Cambrian) arc magmatism in the bitlis massif, SE Turkey: magmatism along the developing northern margin of Gondwana. Tectonophysics 473, 99–112.
Whitney, D.L., Evans, B.W., 2010. Abbreviations for names of rock forming minerals. Am. Mineral. 95, 185–187.
Xiao, L., Clemens, J.D., 2007. Origin of potassic (C-type) adakite magmas: experimental and field constraints. Lithos 95, 399–414.
Xiong, X.L., Adam, J., Green, T.H., 2005. Rutile stability and rutile/melt HFSE partitioning during partial melting of hydrous basalt: implications for TTG genesis. Chem. Geol. 218, 339–359.